

1 [Investigation of the extreme wet-cold compound events changes between 2025-2049 and](#)
2 [1980-2004 using regional simulations in Greece](#)

3 ["Extreme wet-cold compound events investigation under climate change in Greece"](#)

4 Iason Markantonis^{1,2}, Diamando Vlachogiannis¹, Athanasios Sfetsos¹, Ioannis Kioutsioukis²

5 ¹Environmental Research Laboratory, NCSR “Demokritos”, 15341 Agia Paraskevi, Greece

6 ²University of Patras, Department of Physics, University Campus 26504 Rio, Patras, Greece

7 *Correspondence to:* Iason Markantonis (jasonm@ipta.demokritos.gr)

8 **Abstract.** This paper aims to study wet-cold compound events (WCCEs) ~~in over~~ Greece for the wet and
9 cold season November-April, ~~since these events may affect directly human activities for short or longer~~
10 ~~periods as no similar research has been conducted for the country studying the past and future~~
11 ~~development of these compound events.~~ WCCEs are divided in two different ~~daily~~ compound events
12 (~~Maximum Temperature (TX-) -Accumulated Precipitation (RR-)~~) and (~~Minimum Temperature (TN-)~~
13 ~~- Accumulated Precipitation (RR)~~) and two different approaches using fixed ~~thresholds~~ (RR over 20
14 mm/day and Temperature under 0 °C) ~~and percentile (RR over 95th and Temperature under 5th)~~
15 ~~thresholds~~. Observational data from the Hellenic National Meteorology Service (HNMS) and
16 simulation data from reanalysis and ~~EUROCORDEX~~EURO-CORDEX models were used in the study
17 for the historical period 1980-2004. ~~The Ensemble mean of the s~~imulation datasets from projection
18 models were employed for the near future period (2025-2049) to study the impact of climate change on
19 the occurrence of WCCEs under ~~RCP~~Representative Concentration Pathways (RCPs) 4.5 and 8.5
20 scenarios. Following data processing and validation of the models, the potential changes in the
21 distribution of WCCEs in the future were investigated based on the projected and historical
22 simulations. WCCEs determined by fixed thresholds were mostly found over high altitudes with ~~TN-~~
23 ~~RR events exhibiting~~ a future tendency to reduce particularly under RCP 8.5 ~~scenario and TX-RR~~
24 ~~exhibiting similar reduction of probabilities for both scenarios. On the other hand, WCCEs obtained~~
25 ~~with percentile thresholds, were distributed mostly in Eastern Greece and Crete while their changes~~
26 ~~differed significantly among models.~~

27

28 1. Introduction

29

30 Extreme weather events and their linkage to climate change is a matter of high concern for many
31 scientific groups (Zanocco et al., 2018; Konisky et al., 2016; Curtis et al., 2017). In the last decade
32 numerous scientific ~~studies~~researches focused on the causes, the frequency and impacts of extreme
33 compound events (e.g. Aghakouchak et al., 2020; Singh et al., 2021; Sadegh et al., 2018; Zscheischler
34 et al., 2017; Zscheischler and Seneviratne, 2017; Zscheischler et al., 2018). As mentioned in ~~the~~
35 Intergovernmental Panel on Climate Change report on ‘Managing the risks of extreme events and
36 disasters to advance climate change adaptation’ (IPCC SREX) (Ref 7, p. 118) compound events are
37 defined as: (1) two or more extreme events occurring simultaneously or successively, (2) combinations
38 of extreme events with underlying conditions that amplify the impact of the events, or (3) combination
39 of events that are not themselves extremes but lead to an extreme event or impact when combined.~~The~~
40 contributing events can be of similar (clustered multiple events) or different type(s) (Leonard et al.,
41 2014).

42 Recent studies have been conducted on the examination of wet-cold compound events (WCCEs) that
43 concern monthly extreme values of temperature and precipitation and the correlation of these variables
44 (Lemus-Canovas, 2022; Chukwudum and Nadarajah, 2022; Lhotka and Kyselý, 2021; Wu et al., 2019).

45 The purpose of this article is the study of extreme ~~wet cold compound events~~ (WCCEs) on daily basis
46 in Greece during the historical period (1980-2004) and how ~~the~~ the occurrence of these events will be
47 affected by climate change. ~~using projection data from and~~ It has been reported that WCCEs affect the

Μορφωτοίσεις: Γραμματοσειρά: (Προεπιλεγμένη)
Times New Roman, Όχι Πλάγια

Μορφωτοίσεις: Γραμματοσειρά: (Προεπιλεγμένη)
Times New Roman, Όχι Πλάγια

48 region of the Mediterranean Sea, including Greece (Zhang et al., 2021). Studies using only
49 observational data at some locations (Lazogloou and Anagnostopoulou, 2019), or modeled data mostly
50 over the broader region of the Mediterranean Sea (Vogel et al., 2021; Hochman et al., 2021; de Luca et
51 al., 2020), concerning WCCEs have been conducted in the past, not depicting analytically WCCEs in
52 Greece, which is attempted in this work.

Μορφοποίηση: Χρώμα γραμματοσειράς: Κείμενο 1

53 The examined events belong to the first category of the definition of compound events from IPCC since
54 they refer to the simultaneous exceedance of precipitation and temperature thresholds. -WCCEs
55 even may have negative impact on people's lives by causing electricity blackouts, affecting agriculture
56 with heavy snowfall or freezing rain and, blocking transportation because of closed roads, railways or
57 even airports (Houston et al., 2006; Llasat et al., 2014; Vajda et al., 2014). On the other hand, most of
58 the available freshwater in the country comes from melted mountain snow during spring or summer.
59 Finally, eco-systems, especially on mountains, may be harmed/affected by the absence of snow that
60 climate change may cause (Demiroglu et al., 2015; Pestereva et al., 2012; Trujillo et al., 2012; García-
61 Ruiz et al., 2011). Moreover, Athens, a city of more than 4 million inhabitants, experienced in two
62 consecutive years snowstorms (16, 17 February 2021 and 24 January 2022), which caused great
63 problems in road traffic and electricity failures... Historically, such events occur infrequently in the
64 region and it is the first time that snow depth exceeds 15cm twice in a period of eleven months in the
65 city center. At other parts of Greece such events are more frequent, and this is shown in the present
66 study.

Μορφοποίηση: Χρώμα γραμματοσειράς: Κείμενο 1

67 This work extends further and more meticulously the study of Markantonis et al., (2021) about daily
68 minimum temperature and accumulated precipitation WCCEs. The motivation is the absence of such
69 similar study concerning the country, with few exceptions that used only observational data at some
70 locations (Lazogloou and Anagnostopoulou, 2019), or modeled data mostly over the broader region of
71 Mediterranean Sea lacking detailed analysis for Greece (Vogel et al., 2021; Hochman et al., 2021; de
72 Luca et al., 2020). The first/greatest part of the study concerns the historical period between 1980 and
73 2004, because of the availability of quality controlled daily observational data for minimum
74 temperature (TN), maximum temperature (TX) and accumulated precipitation (RR). Hence, for that
75 period, we use observational data from 21 Hellenic National Meteorological Service (HNMS) stations,
76 to for the validation of EURO-CORDEX Regional Climate Models (RCMs), provided by the
77 Copernicus Climate Change Service of EUS-Copernicus Program and the projection model dataset
78 produced in-house. In addition to the models, two reanalysis products are included, as the closest to
79 true past climate conditions in regions with no or scarce observations (Moalafhi et al., 2016). More
80 information about the observational and model datasets is shown/presented in Section 2. Section 3
81 highlights the applied methodology while Section 4 presents displays WCCEs observed in stations and
82 station cells of the models and Section 5 contains Reanalysis and projections Ensemble mean the
83 comparison of model data WCCEs probabilities spatial distribution for the historical period with
84 observations. Section 5.6 details the results about the difference in WCCEs probabilities between the
85 historical and for the historical period and the projected changes by each model for the near future
86 period between 2025 and 2049 for two greenhouse gas concentration scenarios, RCP 4.5 and RCP 8.5.

Μορφοποίηση: Χρώμα γραμματοσειράς: Κείμενο 1

87 88 2. Data

89

90 In this Section we present the datasets that provide the observational and simulation data produced by
91 projection and reanalysis models.

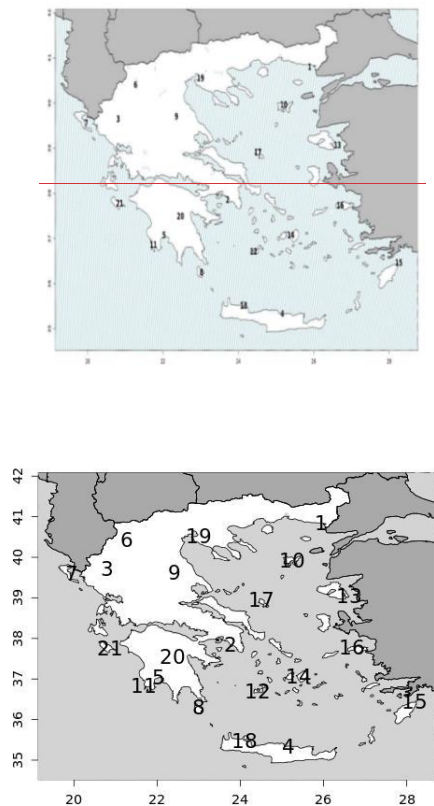
92 1. HNMS observations

93

94 HNMS provides freely observational data from 21 stations for the purpose of scientific research.
95 (<http://www.emy.gr/emy/el/services/paroxi-ipiresion-elefthera-dedomena>). The data have been
96 formally evaluated by HNMS and the timeseries show no missing or distorted values. In particular, the

97 timeseries available for the historical period 1980-2004 have a 3-hour temporal resolution and from
98 these values we have extracted the daily values of TN, TX and RR. Figure 1 shows the position of the
99 stations while Table A1 of Appendix A provides details on the characteristics of the stations. We have
100 used the observational data to validate the model datasets ~~with regard to~~regarding the WCCEs for the
101 historical period.

102
103



104
105 **Figure 1:** Map of HNMS stations. The numbers correspond to those in Table A1 (Appendix A).
106
107

Μορφοποίησε: Γραμματοσειρά: 11 στ.

108 2.2 Reanalysis models

109 We have used two reanalysis models due to the lack of spatially and temporally complete direct
110 observations, to study more consistently the WCCEs in Greece in the historical period. The first model
111 is the latest available reanalysis product ERA 5 from [ECMWF-European Centre for Medium-Range](#)
112 [Weather Forecasts \(ECMWF\)](#) of spatial resolution ~30km x 30km (Hersbach et al., 2020). The second
113 reanalysis model, built in [the Environmental Research Laboratory \(EREL\)](#) of National Center
114 of Scientific Research ‘Demokritos’ (NCSR-D) WRF_ERA_I, has been produced by dynamically
115 downscaling ERA-INTERIM using the Weather Research Forecast (WRF) model (v3.6.1) from 80km
116 x 80km to 5km x 5km (Politi et al., 2021, 2020, 2018).

Μορφοποίησε: Εσοχή: Αριστερά: 0 εκ.

117

4. 2.3 GCM / RCM models

To observe possible alterations of wet cold compound eventsWCCEs occurrence probability in the future period 2025-2049 compared to the historical period, we employed data from RCM simulations driven by GCMs. In this regard, we obtained data from 5 models included in the EURO-CORDEX initiative provided by the Copernicus Program. All chosen Euro-CORDEX models with available daily data were selected because they have at the finest spatial resolution of 0.11° x 0.11° and available daily data for both RCP scenarios and have been tested in (Cardoso et al., 2019). Information on the regional and parent models and their acronyms used herewith is given in Table 1. In addition to the EURO-CORDEX model data, we have used dynamically downscaled data from the EC-EARTH GCM to high spatial resolution of 5km x 5km for the area of Greece using WRF (Politi et al., 2020, 2022).

128

Institution	Reference	Regional Model	Forcing model	Acronym	Resolution (°)
Météo-France / Centre National de Recherches Météorologiques	(Spiridonov et al., n.d.)	ALADIN63	CNRM-CERFACS-CNRM-CM5	CNRM	0.11
Koninklijk Nederlands Meteorologisch Instituut	(van Meijgaard et al., 2008)	KNMI-RACMO22E	ICHEC-EC-EARTH	KNMI	0.11
Climate Limited-Area Modelling Community	(Rockel et al., 2008)	CLMcom-CLM-CCLM4-8-17	MOHC-HadGEM2-ES	CLMcom	0.11
Swedish Meteorological and Hydrological Institute	(Samuelsson et al., 2016)	SMHI-RCA4	MPI-M-MPI-ESM-LR	SMHI	0.11
Danish Meteorological Institute	(Christensen, 2006)	DMI-HIRHAM5	NCC-NorESM1-DIM	DMI	0.11
EREL (NCSRDI	(Politi et al. 2020, 2022)	ARW-WRF	EC-EARTH	WRF_EC	0.05

129

130 Table 1: EURO-CORDEX and EREL-NCSRDI simulation models information.

131

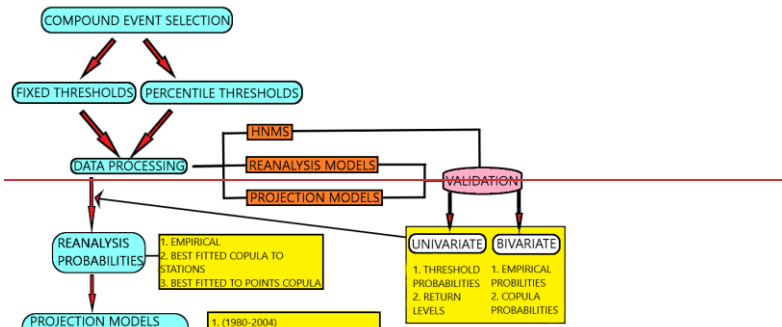
3. Methodology

The process we followed in this work is briefly presented in the flowchart of Figure 2. The light blue steps form the main flow of the approach that mainly include the selection of the compound events based on threshold criteria, validation of the obtained compounds against observational data, and calculation of their occurrence probabilities. The models' validation part is a previous step to the exhibition of modeled data and is added on the data processing step. At the validation step we also compare univariate 20 year return levels using two different approaches, Peaks Over Threshold (POT) and Block Maxima or Minima (BM), further described in section 4.2.2. The calculated probabilities of WCCEs using all models in the historical period have been validated against observations. The yellow boxes describe the results displayed at each step.

132 Μορφοποιήθηκε: Εσοχή: Αριστερά: 1,27 εκ., Χωρίς κουκίδες ή ορίθμηση

Μορφοποίησε: Γραμματοσειρά: 11 στ.

132 Μορφοποιήθηκε: Εσοχή: Αριστερά: 1,27 εκ., Χωρίς κουκίδες ή ορίθμηση



142

143 **Figure 2: WCCEs methodology process flowchart.**

144 The first step in this study is the validation of the projection and reanalysis models against
 145 observations. Moreover, the ensemble of the 6 projection models is also exhibited. We choose as the
 146 Ensemble resolution that of the CORDEX models since 5 of them share the same spatial resolution.
 147 The only model in need of regridding is WRF EC. We follow the nearest neighbor method to upscale
 148 WRF EC from 5 km to 11 km

Μορφοποιήθηκε: Πλήρης

149 In the later sections, In addition, we use box-plots to depict the ability of the models to simulate
 150 observational data WCCEs probabilities for the historical period at the cells that include meteorological
 151 stations. The box-plots consist of the colored box, where in the band near the middle of the box is the
 152 median, the bottom and top of each color box are the 25th (Q1) and 75th Σφέλμα! Η αναφορά της
 153 υπερ σύνδεσης δεν είναι έγκυρη (Q3) percentile (BL) percentile. The lower limit of the whisker
 154 (LLW) is calculated by LW= Q1-1.5*BL and the endsupper limit (ULW) by UW= Q3+1.5*BL. The
 155 length of the whiskers are the 1.5 times(WL) is calculated as the difference between the 25thULW and
 156 LLW75th Σφέλμα! Η αναφορά της υπερ σύνδεσης δεν είναι έγκυρη (WL). Any value out of
 157 this range is marked by a black point in the plot. The validation is conducted after the elevation bias
 158 correction of temperature at the cells of the models containing the stations. The cells of the stations are
 159 found using the nearest neighbor approach and the temperature bias correction temperature is the
 160 following:

Μορφοποίησε: Εκθέτης

Μορφοποίησε: Εκθέτης

Μορφοποίησε: Αγγλικά (Ηνωμένων Πολιτειών)

$$T_e = T_m + 0.06*(H_m - H_s) \quad (1)$$

161 In equation (1) T_e is the temperature of the cell after the elevation bias correction, T_m the temperature
 162 provided by the model, H_m the cell elevation and H_s the elevation of the HNMS station.

Μορφοποίησε: Δείκτης

Μορφοποίησε: Δείκτης

Μορφοποίησε: Δείκτης

Μορφοποίησε: Δείκτης

Μορφοποίησε: Δείκτης

Μορφοποίησε: Δείκτης

164 3.1 Compound event selection

165 According to HNMS the meteorological year can be split into two climate periods
 166 (<http://emy.gr/emy/el/climatology/climatology>). The cold and wet period extends on average from mid-
 167 October to the end of March, and the warm-dry period occurs during the rest of the year. Since the
 168 study is focused on the extreme WCCEs, we examine the period between November and April, since
 169 according to HNMS observations, April exhibits lower temperatures than October and more rainy days.
 170 Moreover, it is not uncommon for the northern parts of Greece, and especially mountainous areas, to be
 171 affected by snowfalls during April. This leads to the creation of a timeseries of 4532 daily values for
 172 the historical period and 4531 for the future period. The only exception is CLMcom which considers
 173 that each month is consisted by 30 days, thus leading to 4500 values for each period. Also, DMI
 174 considers that a calendar year has 365 days, thus each period examined has 4525 values. The near-
 175 neighbour approach revealed the nearest to the station grid cell.

Μορφοποίησε: Δείκτης

Μορφοποίησε: Δείκτης

Μορφοποίησε: Δείκτης

Μορφοποίησε: Δείκτης

Μορφοποίησε: Δείκτης

Μορφοποίησε: Δείκτης

177 The WCCEs, which are examined on daily basis, are divided in two types of synchronous events, TX-
 178 RR and TN-RR and studied using ~~two different approaches~~, (1) the percentile threshold and (2) the
 179 fixed threshold approach (Table 2). For the first method the thresholds are the 95th percentile of RR
 180 distribution and the 5th percentile of TN and TX distribution. This approach examines the threshold for
 181 each variable at each station or grid point. This second approach considers the fixed threshold of 20
 182 mm/day for RR and 0 °C for TN and TX for all stations or grid points, as recommended by the
 183 Commission for Climatology (CCI), the World Climate Research Programme (WCRP) of the Climate
 184 Variability and Predictability Component (CLIVAR) project and the Expert Team for Climate Change
 185 Detection and Indices (ETCCDI). TN equal to or under 0 °C indicates Frost Days (FD), while TX equal
 186 or under 0 °C Iced Days (ID) (Fonseca et al., 2016). Firstly, we compare the univariate exceedance
 187 probabilities and then the bivariate ones. The difference between the two methods is that the percentile
 188 approach calculates the probability that an event considered extreme for the study area occurs, while
 189 the second that an event considered already extreme occurs. The thresholds examined have been
 190 proposed in various works/studies for both univariate and bivariate cases studying extreme events
 191 (Raziee et al., 2014; Tošić and Unkašević, 2013; Anagnostopoulou and Tolika, 2012; Pongrácz et al.,
 192 2009; Kundzewicz et al., 2006; Moberg et al., 2006).

Μορφοποίηση: Χρώμα γραμματοσειράς; Κείμενο 1

THRESHOLDS	RR	TN	TX	WCCE
FIXED	>= 20 mm/day (RR20)	<= 0 °C (FD) (TN5p)	<= 0 °C (ID) (TX5p)	1. (RR20-FD) 2. (RR20-ID)
PERCENTILE	>= 95 th (RR95p)	<= 5 th (TN5p)	<= 5 th (TX5p)	1. (RR95p-TN5p) 1. (RR95p-TX5p)

Μορφοποίηση: Χρώμα γραμματοσειράς; Κείμενο 1

Μορφοποιημένος πίνακας

193
194 **Table 2: Univariate thresholds and the compound events examined in the study.**

Μορφοποίηση: Γραμματοσειρά: 11 στ.

195
196 **3.2 WCCEs probability calculation**

197 The WCCEs probabilities are calculated applying two different methods. The first is the empirical
 198 approach counting the events from the timeseries and dividing by the total number of days to find the
 199 percentage (%) of the occurrence probability. For the second method, we use the copula approach for
 200 the HNMS observations and models comparison and to map the differences of the two methods for the
 201 reanalysis and projection model data. Compared to copula, an empirical method has a higher
 202 uncertainty when calculating the probability of extreme events (Hao et al., 2018; Tavakol et al., 2020;
 203 Zscheischler and Seneviratne, 2017). The purpose of using two different methods is to
 204 investigate/examine whether the copula method underestimates or overestimates the WCCEs.

205 The best fitting copula selection for each timeseries is examined done using the R programming
 206 language function BiCopSelect as suggested in (Zhou et al., 2019), included in the package
 207 VineCopula (Schepsmeier et al., 2013). The appropriate bivariate copula for each dataset is chosen, by
 208 the function, from a multitude of 40 different copula families using the Akaike Information Criterion
 209 (AIC) (Akaike, 1974) and Bayesian Information Criterion (BIC) (Schwarz, 1978), and the copula
 210 chosen for each station and model dataset is shown in Appendix B (Tables B1 and B2). Copulas are
 211 used in plenty of studies that investigate the dependence between two different climate variables and
 212 the joint probability of compound events (Tavakol et al., 2020; Dzupire et al., 2020; Pandey et al.,
 213 2018; Cong and Brady, 2012; Abraj and Hewaarachchi, 2021).

214 As mentioned in Nelsen, (2007), a bivariate copula is a bivariate distribution function where margins
 215 are uniform on the unit interval [0, 1]. A bivariate copula is a map $C:[0,1]^2 \rightarrow [0,1]$ with $C(u,1)=u$ and
 216 $C(1,v)=v$. Let X and Y be random variables with a joint distribution function $F(x,y)=Pr(X \leq x, Y \leq y)$ and
 217 continuous marginal distribution functions $F_1(x)=Pr(X \leq x)$ and $F_2(y)=Pr(Y \leq y)$, respectively. By Sklar's
 218 theorem (Sklar, 1959), one obtains a unique representation
 219

$$220 \quad F(x,y) = C\{F_1(x),F_2(y)\} \\ 221 \quad (2)(4)$$

222 For the two random variables of X (e.g., precipitation) and Y (e.g., temperature) with cumulative
223 distribution functions (CDFs) $F_1(x)=\Pr(X>=x)$ and $F_2(y)=\Pr(Y<=y)$, the bivariate joint distribution
224 function or copula (C) can be written as:

$$225 \quad F(x,y) = \Pr(X>=x, Y<=y) = C(u,v) \\ 226 \quad (3)(2)$$

227 ~~Besides copula probabilities, we also show the Kendall rank correlation and tail dependence (γ)~~
228 between the variables (RR-TN) and (RR-TX) to examine the dependence between the variables over
229 all the range and tails of the distribution.

230 ~~The Kendall rank correlation coefficient evaluates the degree of similarity between two sets of ranks~~
231 given to a same set of objects (Abdi, 2007) and we prefer it from other correlation types because it
232 provides a distribution free test of independence and a measure of the strength of dependence between
233 two variables. Kendall's tau (τ) is given by Eq. 3, and has a range [-1, 1].

$$234 \quad \tau = (N_c - N_d) / (n*(n-1) / 2) \quad (3)$$

235 where, N_c is the number of concordant pairs and N_d the number of discordant pairs.

236 ~~Tail dependence describes the limiting proportion that one margin exceeds a certain threshold given~~
237 that the other margin has already exceeded that threshold that has a range [0, 1]. In R, we use the
238 function taildep from package extRemes (Gilleland and Katz, 2016) for the threshold $u=0.95$ to
239 calculate Chi (γ). Chi is calculated by:

$$240 \quad \text{chi}(u) = \Pr[Y > G^{-1}(u) | X > F^{-1}(u)] = \Pr[V > u | U > u], \quad (4)$$

241 where $(U, V) = (F(X), G(Y))$ i.e., the copula.

242

243 4. WCCEs assessment in HNMS stations

244 1. Results in observation locations

245

246 In this section, ~~models are validated against observations both for the empirical and the copula method~~.
247 WCCEs probabilities for each station and model are presented in supplementary material. BIAS and
248 RMSE along with Critical Success Index (CSI) are used for the validation. CSI is calculated as:
249 $CSI = A / (A + B + C)$. A, B and C symbolize elements from the contingency table (Table 2) that occur from
250 comparing zero and non-zero probabilities in stations with the corresponding model cells. Also, total
251 number of events calculated for both methods from observational data are presented in each station,
252 we firstly examine the dependence between the variables based on the HNMS data and using these data
253 we calculate the probability of WCCEs applying both empirical and copula approaches. Then, we use
254 the HNMS data to validate both reanalysis and projection models during the historical period.

255

"EVENT"=POSITIVE PROBABILITY		OBSERVATION EVENT	
MODEL	YES	YES	NO
		A	B
EVENT	NO	C	D

256 **Table 2: Contingency table where "A"** is the number of event forecasts that correspond to event
257 observations, or the number of hits, Entry "B" is the number of event forecasts that do not
258 correspond to observed events, or the number of false alarms, Entry "C" is the number of no-
259 event forecasts corresponding to observed events, or the number of misses, Entry "D" is the

Με σχόλια [jm1]: Να βγαλω το κενταλ

Μορφοποίηση: Γραμματοσειρά: Times New Roman, 10 στ., Έντονα

Μορφοποιήθηκε: Με αριθμηση + Επίπεδο: 1 + Στυλ αριθμησης: 1, 2, 3, ... + Έναρξη από: 4 + Στοίχιση: Αριστερά + Στοίχιση: 0,63 εκ. + Εσοχή: 1,27 εκ.

Μορφοποιήθηκε: Εσοχή: Αριστερά: 1,27 εκ., Χωρίς κουκίδες ή αριθμηση

Μορφοποίηση: Γραμματοσειρά: Όχι Έντονα

Μορφοποιήθηκε: Εσοχή: Αριστερά: 1,27 εκ.

Μορφοποίηση: Γραμματοσειρά: 10 στ.

Μορφοποίηση: Γραμματοσειρά: 10 στ.

Μορφοποιήθηκε: Στοιχισμένο στο κέντρο

Μορφοποίηση: Γραμματοσειρά: 10 στ.

Μορφοποίηση: Γραμματοσειρά: 10 στ., Έντονα, Ελληνικά

Μορφοποίηση: Γραμματοσειρά: 10 στ., Έντονα

Μορφοποίηση: Γραμματοσειρά: 10 στ., Έντονα, Ελληνικά

Μορφοποιημένος πίνακας

Μορφοποιήθηκε: Στοιχισμένο στο κέντρο

Μορφοποίηση: Γραμματοσειρά: 10 στ.

Μορφοποίηση: Γραμματοσειρά: 10 στ., Έντονα

Μορφοποίηση: Αγγλικά (Ηνωμένων Πολιτειών)

260 number of no-event forecasts corresponding to no events observed, or the number of correct
261 rejections.

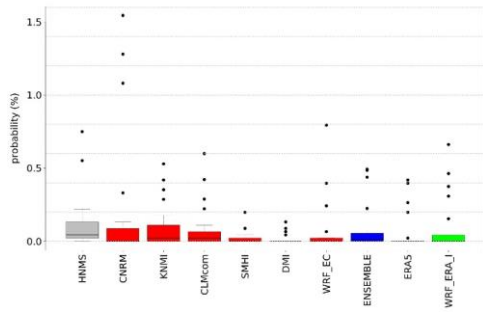
262

263 **1. HNMS WCCE climatology**

264 **4.1 RR20FD**

265 Probability values for each station are presented in Supplementary (Tables S1-S4) as well as the
266 contingency tables (Tables S7-S10) from which CSI is calculated. ERA5 and WRF ERA I are
267 reanalysis products and exhibited for comparison reasons. The copulas selected by Bicopselect for each
268 observational and modeled timeseries are also presented in Supplementary (Tables S5-S6).

269



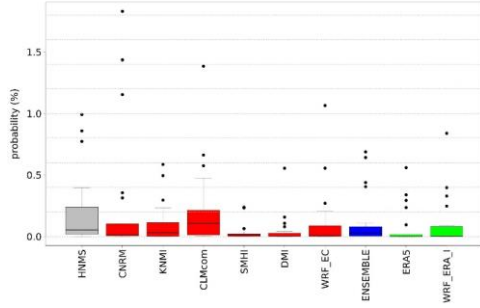
270

271 **Figure 2:** Box-plot presenting RR20FD empirical method probabilities for observations and
272 models.

	HNMS	CNRM	KNMI	CLMcom	SMHI	DMI	WRF_EC	ENSEMBLE	ERA5	WRF_E
MEAN	0.1177	0.2217	0.0977	0.0899	0.0252	0.0158	0.0935	0.0906	0.0620	0.098
SD	0.1912	0.4641	0.1600	0.1622	0.0480	0.0364	0.2034	0.1674	0.1347	0.188
BIAS	-0.1040	0.0199	0.0277	0.0924	0.1019	0.0242	0.0270	0.0557	0.0557	0.018
RMSE	0.3410	0.1216	0.0929	0.1718	0.2029	0.1131	0.0989	0.1273	0.1273	0.111
COR	0.7958	0.7689	0.8804	0.9183	0.4000	0.8371	0.8604	0.7949	0.7949	0.823
CSI	0.4762	0.5500	0.5000	0.4000	0.1905	0.3500	0.6842	0.2381	0.2381	0.400

273 **Table 3:** Table exhibiting mean (MEAN) station RR20FD empirical probabilities probabilities
274 (%) for observations and models, standard deviation (SD), bias (BIAS), rmse (RMSE), Pearson
275 correlation (COR) and CSI of models against observations.

276



277

Figure 3: Box-plot presenting RR20FD copula method probabilities for observations and models.

	<i>HNMS</i>	<i>CNRM</i>	<i>KNMI</i>	<i>CLMcom</i>	<i>SMHI</i>	<i>DMI</i>	<i>WRF EC</i>	<i>ENSEMBLE</i>	<i>ERA5</i>	<i>WRF ER</i>
<i>MEAN</i>	0.2032	0.2592	0.1030	0.2096	0.0341	0.0495	0.1130	0.1281	0.0742	0.099
<i>SD</i>	0.3014	0.5283	0.1686	0.3323	0.0689	0.1232	0.2558	0.2160	0.1524	0.205
<i>BIAS</i>	-0.0560	0.1002	-0.0064	0.1691	0.1537	0.0902	0.0751	0.1290	-0.103	0.169
<i>RMSE</i>	0.2493	0.1891	0.2672	0.2962	0.2743	0.1573	0.1320	0.2129	0.923	0.700
<i>COR</i>	0.9671	0.9079	0.6307	0.8053	0.6979	0.9004	0.9610	0.9140	0.5238	0.5238
<i>CSI</i>	0.8889	0.9444	1.0000	0.9474	0.6190	0.7500	1.0000	0.5238	0.5238	0.5238

278

Table 4: Table exhibiting mean (MEAN) RR20FD copula probabilities station probabilities (%) for observations and models, standard deviation (SD), bias (BIAS), rmse (RMSE), Pearson correlation (COR) and CSI of models against observations.

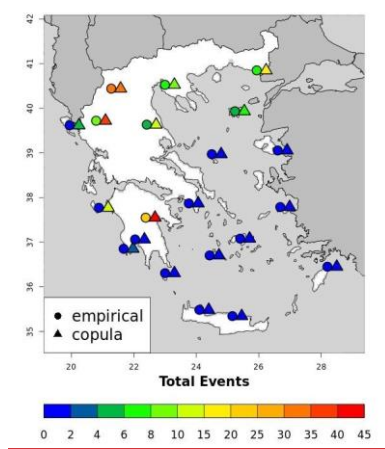
279

280
281
282
283

Figure 3 presents the tail dependence for the two different types of compound events examined. Only two stations in Crete show minor dependence between the variables at the tails of the distributions. Figure 4

284
285
286
287

Figure 4 shows that (RR20-FD) events display higher numbers are located mostly in the mainland, while RR95p-TN5p in the Aegean Sea area. At several stations, there is a difference between the empirical and the copula approach, which in stations usually overestimates the total number of WCCCs.



288

Μορφοποίησε
Μορφοποιημένος πίνακας

Μορφοποίησε

Μορφοποιήθηκε

Μορφοποίησε

Figure 4: Total number of RR20FD WCCEs (1980-2004). Circles symbolize empirical and triangles the copula method.

291 4.2 RR20ID

RR20ID events yield, as expected, lower probabilities than RR20FD events as observed in Figures 5 and 6. Most observations and models yield zero probabilities, hence validation of models for these events is limited. Empirical method exhibits only two stations with events in the historical period for the empirical method (Figure 7).

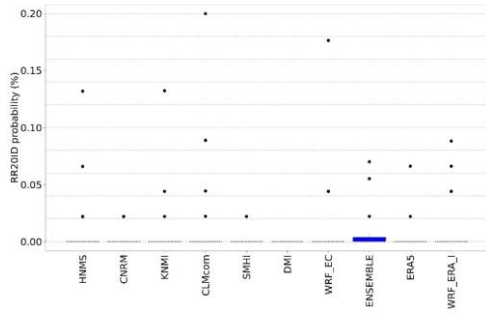
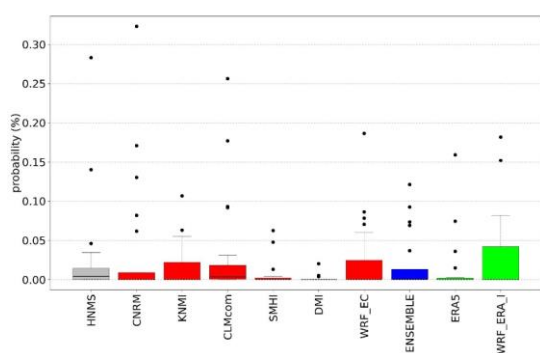


Figure 5: Box-plot presenting RR20ID empirical method probabilities for observations and models.

	<u>HNM5</u>	<u>CNRM</u>	<u>KNMI</u>	<u>CLMcom</u>	<u>SMHI</u>	<u>DMI</u>	<u>WRF EC</u>	<u>ENSEMBLE</u>	<u>ERA5</u>
<u>MEAN</u>	0.0115	0.0032	0.0095	0.0212	0.0011	0.0000	0.0126	0.0079	0.0042
<u>SD</u>	0.9316	0.0079	0.0301	0.0494	0.0048	0.0000	0.0398	0.0191	0.0150
<u>BIAS</u>		0.0084	0.0021	-0.0096	0.0105	0.0115	-0.0011	0.0036	0.0073
<u>RMSE</u>		0.0263	0.0068	0.0280	0.0288	0.0329	0.0330	0.0157	0.0220
<u>COR</u>		0.8185	0.9782	0.8692	0.8738	NA	0.5733	0.9256	0.8149
<u>CSI</u>		0.1429	0.1429	0.1111	0.0476	0.0000	0.1000	0.1667	0.0500

Table 5: Table exhibiting mean (MEAN) RR20ID empirical probabilities station probabilities (%) for observations and models, standard deviation (SD), bias (BIAS), rmse (RMSE), Pearson correlation (COR) and CSI of models against observations.

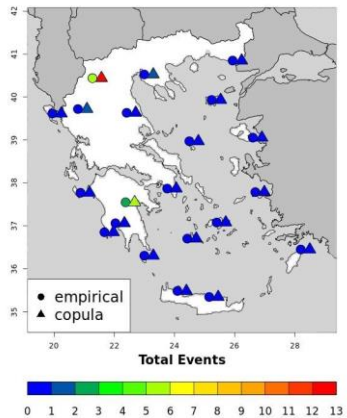


304

Figure 6: Box-plot presenting RR20ID copula method probabilities for observations and models.

	<i>HNMS</i>	<i>CNRM</i>	<i>KNMI</i>	<i>CLMcom</i>	<i>SMHI</i>	<i>DMI</i>	<i>WRF EC</i>	<i>ENSEMBLE</i>	<i>ERAS</i>	<i>WRF EC</i>
<i>MEAN</i>	0.0282	0.0378	0.0169	0.0344	0.0066	0.0017	0.0249	2.040E-02	0.0138	0.027
<i>SD</i>	0.0663	0.0811	0.0303	0.0676	0.0166	0.0046	0.0473	3.640E-02	0.0377	0.052
<i>BIAS</i>	-0.0097	0.0112	-0.0062	0.0215	0.0264	0.0032	0.0078	0.0144	0.000	0.000
<i>RMSE</i>	0.0532	0.0493	0.0598	0.0565	0.0691	0.0489	0.0443	0.0420	0.033	0.033
<i>COR</i>	0.7534	0.7228	0.5861	0.8202	0.2291	0.6594	0.7712	0.8370	0.854	0.854
<i>CSI</i>	0.4000	0.3810	0.7857	0.4737	0.3333	0.4211	0.7857	0.2857	0.35	0.35

305

Table 6: Table exhibiting mean (MEAN) RR20ID copula probabilities station probabilities (%) for observations and models, standard deviation (SD), bias (BIAS), rmse (RMSE), Pearson correlation (COR) and CSI of models against observations.

308

Figure 7: Total number of RR20ID WCCEs (1980-2004). Circles symbolize empirical and triangles the copula method.

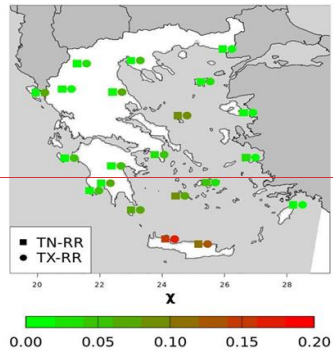
4.3 Observations-models comparison conclusions

The events examined are rare among the stations available for the historical period. Copulas considering the dependence between the variables yield greater probabilities than the empirical method. More stations with non-zero probabilities enable more accurate validation of the models. To minimize uncertainties, smooth extreme underestimations or overestimations of WCCE probabilities that each model yields and because ENSEMBLE shows better consistency among the projection models statistical indices, we use it for further analysis in the study.

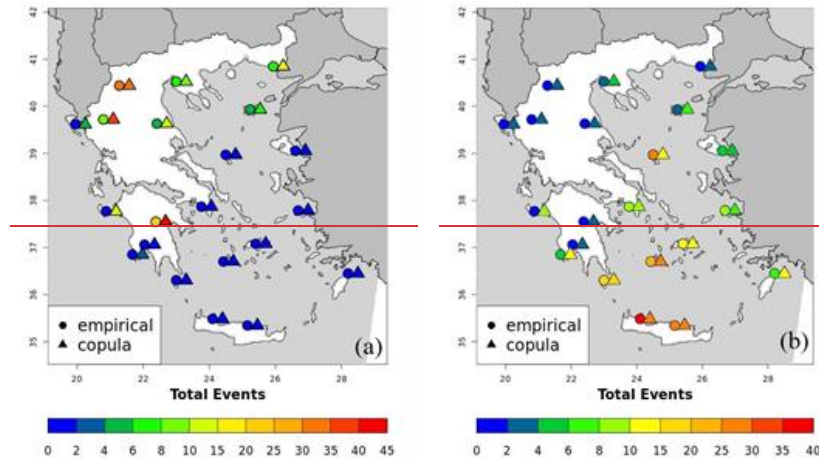
In Figure 5a only two stations show a significant number of RR20 ID events. At the percentile threshold approach (Figure 5b), we observe few WCCEs using the empirical method, while all stations show a significant number of WCCEs using the copula method.

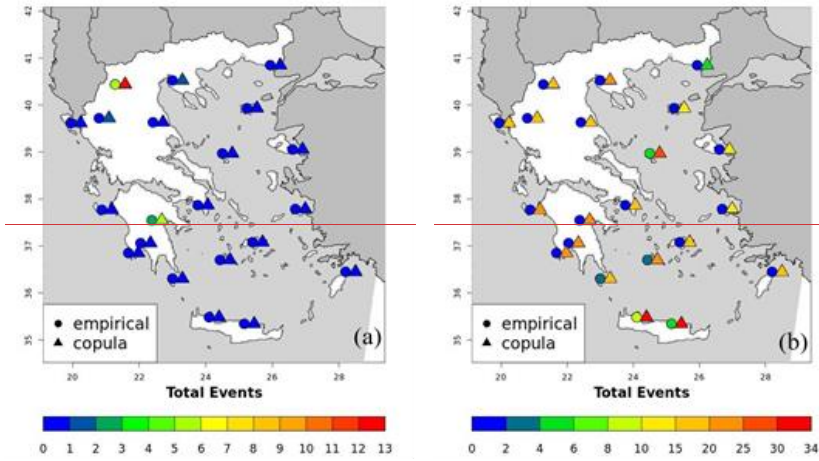
321

322 **Figure 3:** Tail dependence (γ) for TN-RR (squares) and TX-RR (circles).



323



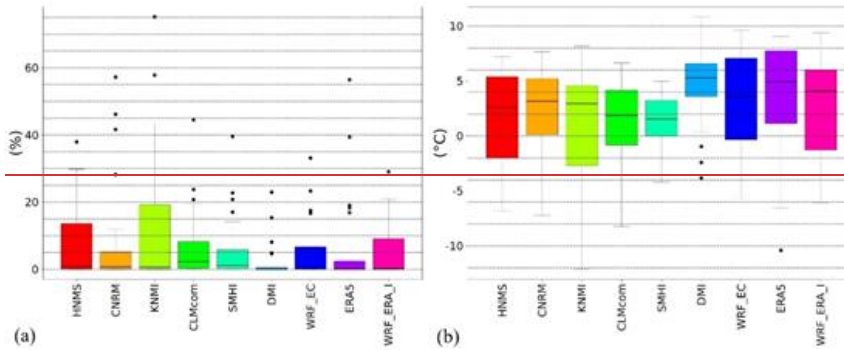


324 **Figure 5:** Total number of WCCEs (1980–2004) for (a) RR20_ID and (b) RR95p_TX5p.

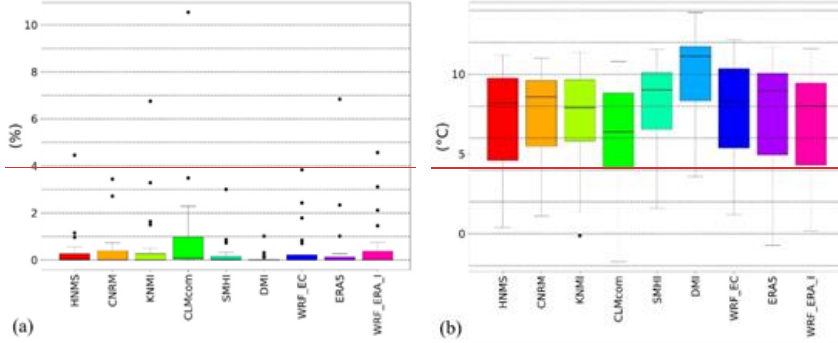
325
326 **2. Univariate validation**

327
328 Both reanalysis and projections models are compared to observational data for each variable and for the
329 WCCEs probabilities. Figures 6–8 present the mean values and the standard deviation for stations and
330 the respective models' grid points. The corresponding values for each station are shown in Tables S1–
331 S3 and S5–S7 from Supplementary material.

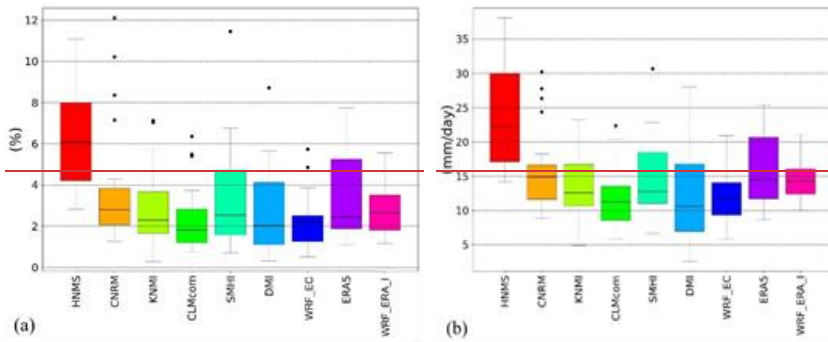
332 **4.2.1 Thresholds & Probabilities**



333 **Figure 6:** Boxplots of (a) FD probability and (b) TN5p threshold.



335 **Figure 7: Boxplots of (a) ID probability and (b) TX5p threshold.**



337 **Figure 8: Boxplots of (a) RR20 probability and (b) RR95p threshold.**

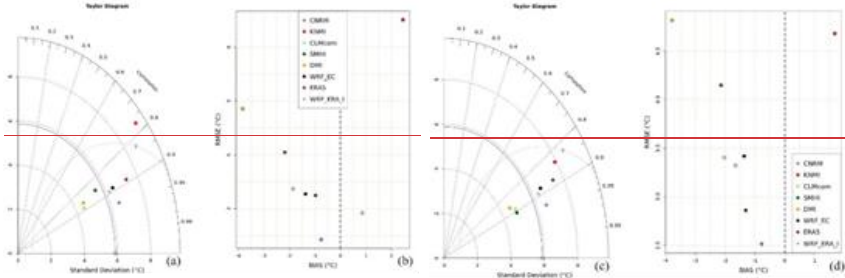
338 For TN and TX (Figures 6 and 7, respectively) seems to be a good concordance of most models mean
 339 values with the HNMS data, although there are differences in the range of BL and WL between the
 340 models. The model that mostly overestimates TX5p and TN5p thresholds is DMI. For RR (Figure 8),
 341 all models underestimate extreme values compared to HNMS with ERA5 being closer to observations.

342 **4.2.2 Return levels**

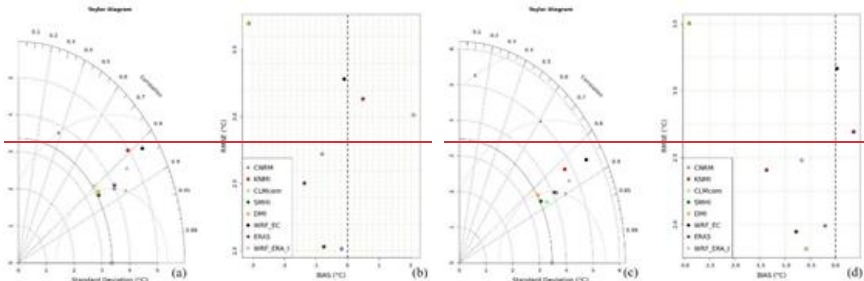
343 Another way to compare extreme values is the calculation of return levels. As mentioned in
 344 methodology we use two approaches, (BM) and (POT). For BM we use the annual maximum or
 345 minimum value of the variable that results in the loss of information, because there is available only
 346 one value per year. BM samples tend to follow the GEV distribution, according to The Fisher-Tippett-
 347 Gnedenko theorem (Fisher and Tippett, 1928; Gnedenko, 1943). For BM we fit the GEV by applying
 348 the method 'lmoments' using the function f gev from R package extRemes.

349 On the other hand, POT has the advantage of examining more values per year with the chosen
 350 condition that the values above the right threshold are considered as extreme (Balkema and Haan,
 351 1974; James Pickands, 1975). The approach is to select as threshold the 90th percentile of the variable
 352 distribution (Bommier, 2014). Also, in order to achieve that each extreme value is independent from
 353 another, we use a conservative 5-day threshold declustering (Coles, 2001), securing that there are no
 354 extreme values affected by the same synoptic system. For POT we fit the Generalized Pareto (GP)
 355 distribution, which corresponds to the tail distribution of the GEV (Goda, 2018). As suggested in

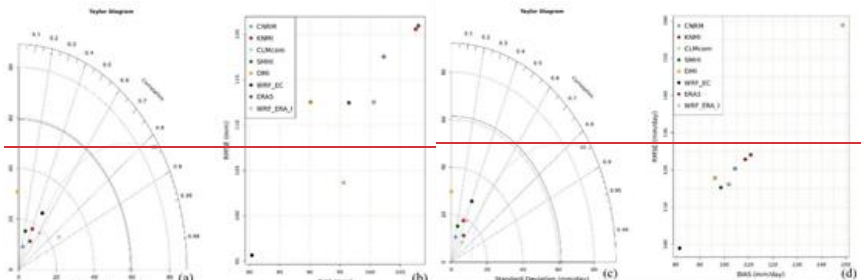
356 Posehlo, (2021), we use Maximum Likelihood Estimation (MLE) as an optimization algorithm to fit
 357 the GP to the declustered timeseries, using again the extRemes package.



358 **Figure 9:** Taylor diagram for TN 20 years return level using (a) POT and (c) BM approach.
 359 RMSE-BIAS plots for (b) POT and (d) BM.



360 **Figure 10:** Taylor diagram for TX 20 years return level using (a) POT and (c) BM approach.
 361 RMSE-BIAS plots for (b) POT and (d) BM.



362 **Figure 11:** Taylor diagram for RR 20 years return level using (a) POT and (c) BM approach.
 363 RMSE-BIAS plots for (b) POT and (d) BM.

364 Figures 9 and 10 show that the CNRM is the model closer to HNMS TN and TX 20 years return level.
 365 Figure 11 yields that WRF_ERA_I has the highest correlation to observations, while WRF_EC the best
 366 RMSE-BIAS relation to observations. The values used to produce Figures 9–11 can be found in Tables
 367 S11–S16 from Supplementary material.

368

369 Bivariate

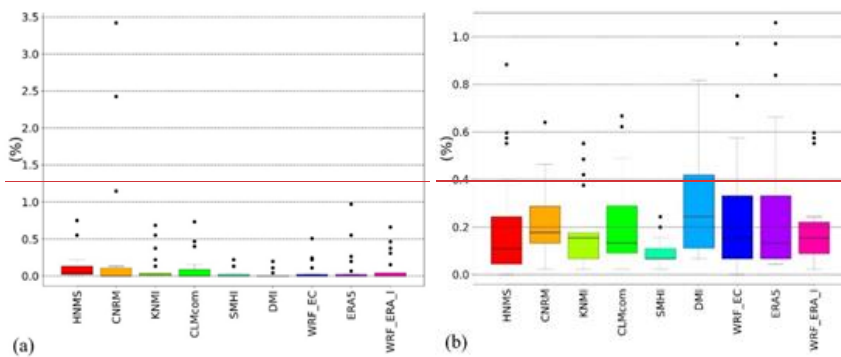
370 3. validation

371 The bivariate validation of the models is conducted by the empirical and copula methods for the
372 WCCEs at the stations. Figures 12 and 13 summarize the results from Supplementary material Tables
373 S4, S5 and S9, S10, respectively.

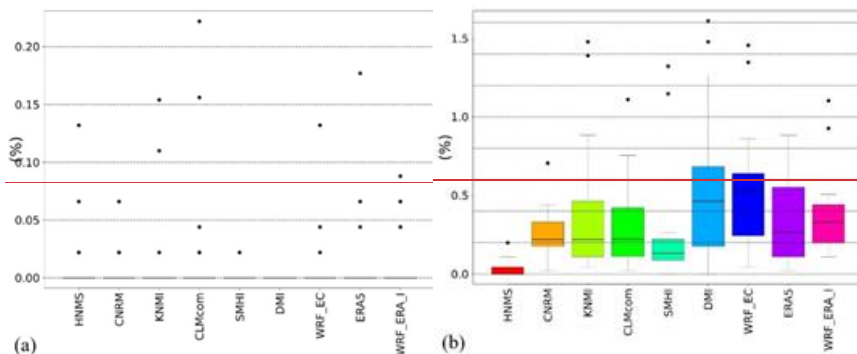
374

375 1. Empirical approach

376



377 **Figure 12:** Boxplots of probabilities for (a) RR20-FD and (b) RR95p-TN5p WCCEs.

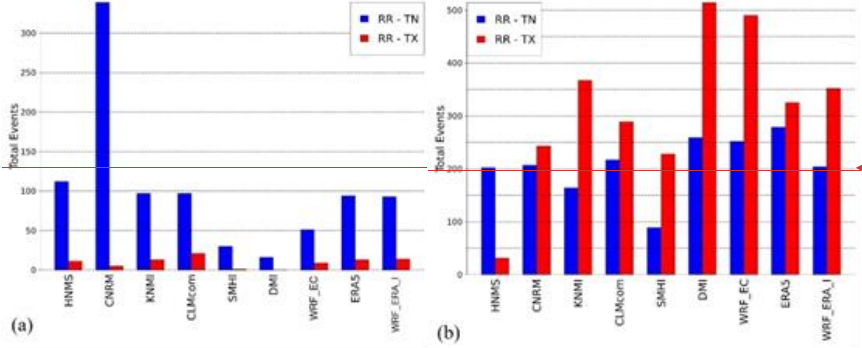


378 **Figure 13:** Boxplots of probabilities for (a) RR20-ID and (b) RR95p-TX5p WCCEs.

379 In Figure 12a, HNMS BL is greater than all models, although a number of models show values greater
380 than the WL of observations, with CNRM yielding the most extreme values, with 3 cases of more than
381 1% probability. RR95p-TN5p events probabilities from models are close or over the mean values and
382 BL of HNMS except for the case of SMHI which shows smaller values (Figure 12b). From Figure 13a
383 we find that RR20 ID events are extremely rare at the locations of the stations with few
384 exceptions. DMI exhibits zero events, while the largest probabilities are exhibited by
385 CLMcom with four non zero probabilities points . In Figure 13b, we see that all models
386 overestimate the probabilities of RR95p-TX5p events with DMI showing the highest
387 probabilities and SMHI the closer to HNMS agreement.

370 **Μορφοποιήθηκε:** Εσοχή: Αριστερά: 1,9 εκ., Χωρίς
371 κουκκίδες ή αριθμηση

375 **Μορφοποιήθηκε:** Εσοχή: Αριστερά: 2,54 εκ., Χωρίς
376 κουκκίδες ή αριθμηση



Μορφοποιήθηκε: Αριστερά

388 **Figure 14:** Bar-plots of total number of WCCEs for (a) fixed and (b) percentile thresholds for the
389 1980-2004 period.

390 In Figure 14, we present a quantitative comparison of the total number of compound events that are
391 counted for all stations and the corresponding grid points for each model. For fixed thresholds, most
392 models show good agreement with the HNMS data except of CNRM which overestimates the amount
393 of total WCCEs for the RR-TN case. Also, SMHI and DMI and to a lesser extent WRF-EC
394 underestimate significantly the number of total events for both types. With the percentile threshold
395 approach all models overestimate the number of WCCEs for the RR-TX case, while for the RR-TN
396 case most models are close to the HNMS total number of WCCEs, except of SMHI which
397 underestimates it.

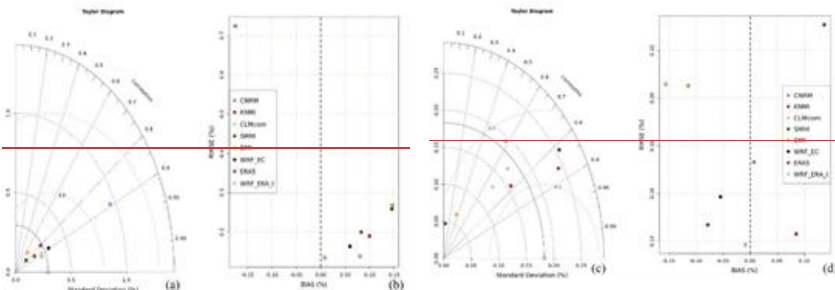
398

399

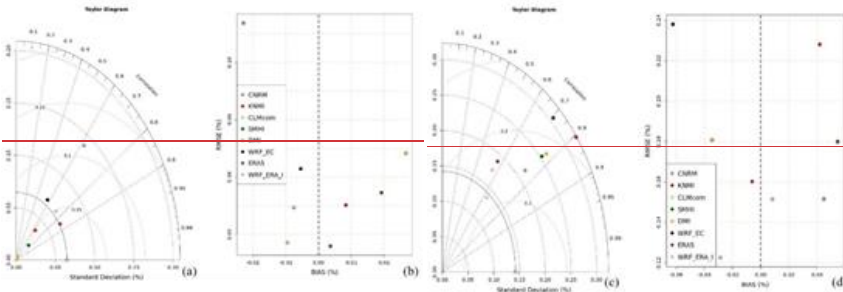
2. Copula approach

400 The best fitted copulas fixed and percentiles probabilities for each model dataset are compared to the
401 respective HNMS station best fitted copula in Figures 15 and 16, respectively. We use Taylor diagrams
402 and RMSE-BIAS plots to observe which models are closer to the WCCEs probabilities calculated for
403 the HNMS data.

Μορφοποιήθηκε: Εσοχή: Αριστερά: 2,54 εκ., Χωρίς κουκίδες ή αρίθμηση



404 **Figure 15:** Taylor diagram of WCCEs copula probabilities for (a) RR20-FD and (c) RR95p-
405 TN5p. RMSE-BIAS plots of WCCEs copula probabilities for (b) RR20-FD and (d) RR95p-TN5p.



406 **Figure 16:** Taylor diagram of WCCEs copula probabilities for (a) RR20-ID and (c) RR95p-TX5p.
 407 **RMSE-BIAS plots of WCCEs copula probabilities for (b) RR20-ID and (d) RR95p-TX5p.**

408 Figures 15 and 16 show that models agree more with observations on fixed thresholds WCCEs than the
 409 percentiles ones, where there is a broader deviation of correlation to observations. Probabilities for
 410 WCCEs are generally close to zero for observations and models, therefore RMSE and BIAS values are
 411 also almost zero. The values for each station are presented analytically in Tables S19-S22 from the
 412 Supplementary material.

413

414

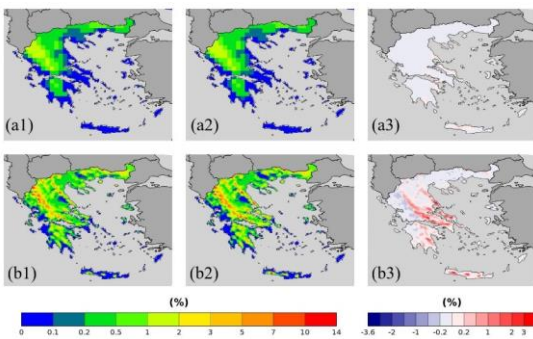
415

416 2. 5. Historical period Models-WCCEs on maps

417 In this section WCCEs spatial distribution probabilities are compared between empirical and copula
 418 methods. This procedure is conducted separately for the two reanalysis products and the Ensemble
 419 mean of the projection models.

420 4. 5.1 Reanalysis

421 ERA5 and WRF ERA I WCCEs spatial distribution probabilities spatial distribution in Greece are
 422 displayed in this section. We display both reanalysis products, although ERA5 is the most recently
 423 developed reanalysis product, we exhibit also WRF ERA I since its much finer spatial resolution is
 424 more appropriate for the complex topography of Greece with many mountains and islands.

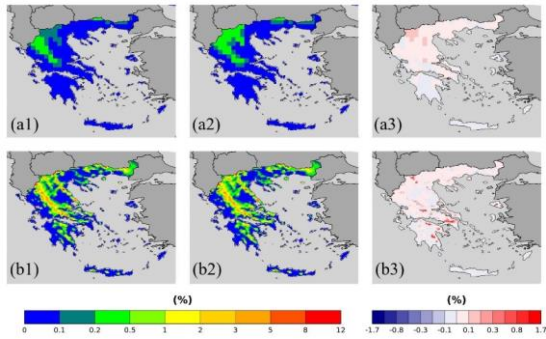


425
 426 **Figure 8:** RR20FD probabilities for (a) ERA5 and (b) WRF ERA I produced by (1) Empirical
 427 and (2) Copula and (3) = (2)-(1).

Μορφοποιήθηκε: Χωρίς κουκίδες ή αριθμηση

Μορφοποιήθηκε: Πλήρης

Μορφοποιήθηκε: Εσοχή: Αριστερά: 1,27 εκ., Χωρίς κουκίδες ή αριθμηση



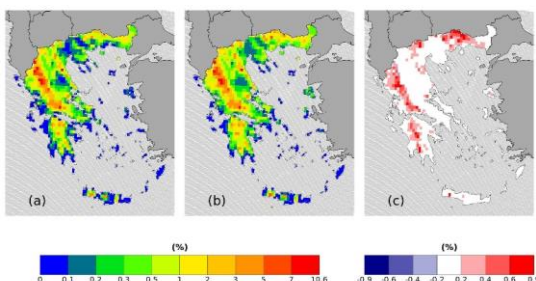
428

429 **Figure 9: RR20ID probabilities for (a) ERA5 and (b) WRF ERA I produced by (1) Empirical
430 and (2) Copula and (3) = (2) –(1).**

431 Both reanalysis products yield greater WCCEs probabilities in Pindus mountains, although due to its
432 finer spatial resolution, WRF ERA I display high probabilities at other mountainous regions located in
433 Crete, Peloponnes, Evia Island and others. Also, in both WCCEs copula method yields higher
434 probabilities, especially for WRF ERA I and the RR20FD case. Moreover, WRF ERA I displays a
435 greater range than ERA5 with RR20FD probabilities reaching 14% and RR20ID 12% compared to 6%
436 and 2% of ERA5 respectively.

437 **5.2 Projections Ensemble**

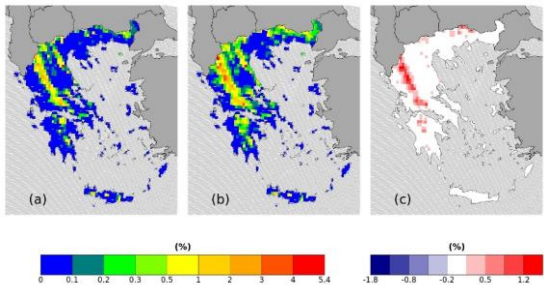
438 Figures 10 and 11 yield that Ensemble mean displays similar to WRF ERA I spatial distribution of
439 WCCEs. RR20FD and RR20ID probabilities reach 10.8% and 5.4% respectively. The copula method
440 yield higher probabilities for both methods in mountainous regions with greater difference displayed
441 for RR20ID events in the Pindus mountain range and RR20FD exhibiting greater spatial distribution in
442 differences between the two methods.



443

444 **Figure 10: RR20FD Ensemble probabilities for (a) Empirical and (b) Copula method. (c)=(b)-(a).**

Μορφωτοίσης: Γραμματοσειρά: Έντονα

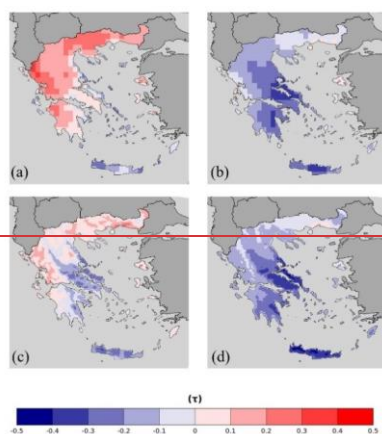


445

446 **Figure 11: RR20ID Ensemble probabilities for (a) Empirical and (b) Copula method. (c)=(b)-(a).**

447

448 Data from reanalysis models provide us with information on the WCCEs for the historical period, at
 449 places with no available observational data. Thus, we will examine the probability of WCCEs using
 450 three different methods for the reanalysis data. (1) The empirical probability method, (2) the probability
 451 calculated by the most common copula from the total of the 21 HNMS stations and (3) the best fitted
 452 copula at each grid point of the model. For comparison, we show the differences between each pair of
 453 methods. The reason to show the second method is to examine its ability to resemble the empirical
 454 method, since it is computationally much faster than method (3). In Tables B1 and B2 of Appendix B it
 455 is shown that the best fitted copula for HNMS timeseries is the Rotated BB8-270 degrees for (TN, RR)
 456 bivariate distribution and the Survival BB8 for (TX, RR) bivariate distribution. In both cases, the
 457 copulas are chosen for 10 out of the 21 stations. In the appendix, the univariate probabilities and
 458 thresholds are also shown. Firstly, we show the Kendall rank correlation (τ) (Figure 17) and then the
 459 tail-dependence (γ) (Figure 18) between the variables. For the sake of brevity, we refer to the three
 460 methods as (A), (B) and (C).



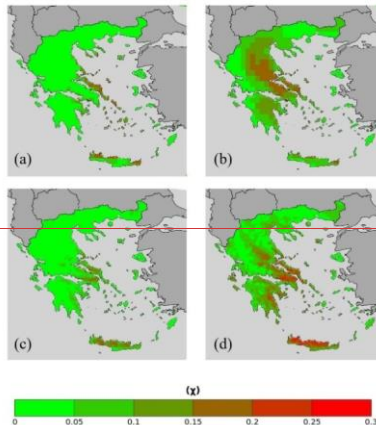
461

462 **Figure 17: Kendall rank correlation (τ) between (a, c) TN-RR and (b, d) TX-RR and (a, b) ERA-5**
463 **and (c, d) WRF-ERA-1.**

Μορφοποίηση: Γραμματοσειρά: Έντονα

Μορφοποίηση: Γραμματοσειρά: Όχι Έντονα

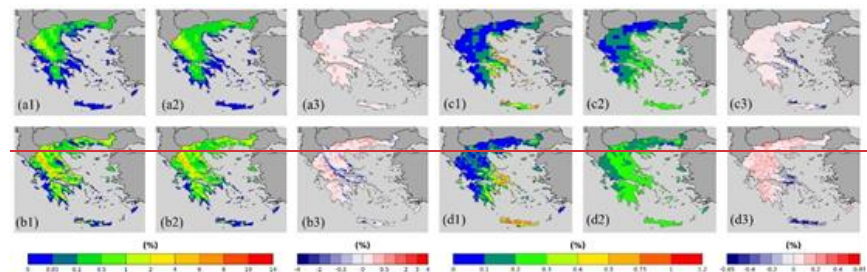
Μορφοποιήθηκε: Πλήρης, Εσοχή: Αριστερά: 0 εκ.



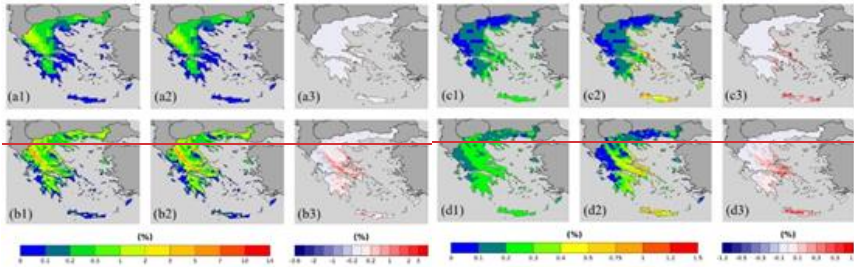
464
465 **Figure 18:** Tail dependence (γ) at 95% between (a, c) TN_RR and (b, d) TX_RR and (a, b) ERA-5
466 and (c, d) WRF_ERA-I.

467
468 Figure 17 shows that there is little correlation between the variables with TN_RR having mostly slight
469 positive correlation (17a, 17c), while more negative correlation reaching to -0.5 is calculated for TX-
470 RR (17b, 17d). From tail-dependence for the 5 % of the distributions in Figure 18, we see that TX_RR
471 (18a, 18c) are more dependent from TN_RR (18b, 18d) in more regions of the map. Values reach up to
472 0.3 mainly for TX_RR in eastern Greece and Crete. Also, Figures S1-S3 in the supplementary material
473 present the univariate thresholds and probabilities for RR, TN and TX using the reanalysis datasets
474 (ERA5 and WRF_ERA-I).

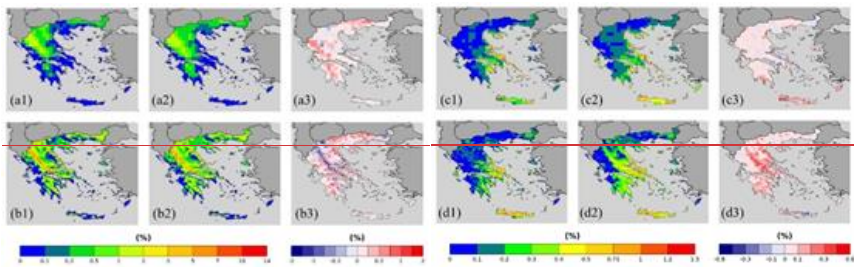
475 1. TN_RR_WCCEs



478 **Figure 19:** (a, b) RR20-FD and (c, d) RR95p-TN5p-WCCEs probabilities. (a, c) ERA-5 and (b, d)
479 WRF_ERA-I. Column (1) is method A, (2) method B and (3)=(2)-(1).



480 **Figure 20:** (a, b) RR20-FD and (c, d) RR95p-TN5p WCCEs probabilities. (a, e) ERA-5 and (b, d)
481 WRF-ERA-I. Column (1) is method B, (2) method C and (3) = (2) – (1).



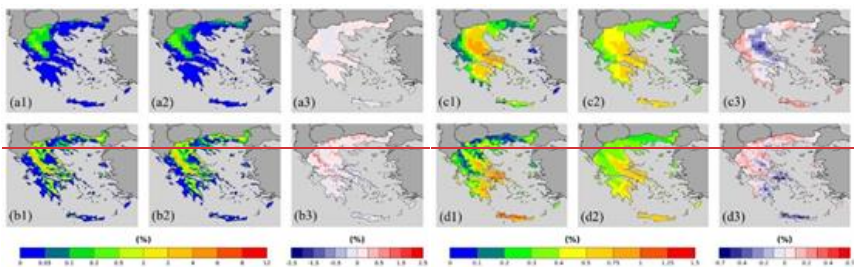
482 **Figure 21:** (a, b) RR20-FD and (c, d) RR95p-TN5p WCCEs probabilities. (a, c) ERA-5 and (b, d)
483 WRF-ERA-I. Column (1) is method A, (2) method C and (3) = (2) – (1).

484 From Figures 19 and 20 we observe that method B underestimates the extreme value probabilities
485 compared to methods A and C. On the other hand, method B exhibits less non-zero values compared to
486 method A. In Figure 21, we see that method C mostly overestimates WCCEs compared to method A,
487 especially for RR95p-TN5p and WRF-ERA-I. RR20-FD events reach at most extreme probabilities of
488 1.4%, while for RR95p-TN5p the highest probabilities range between 1.2% and 1.5%.

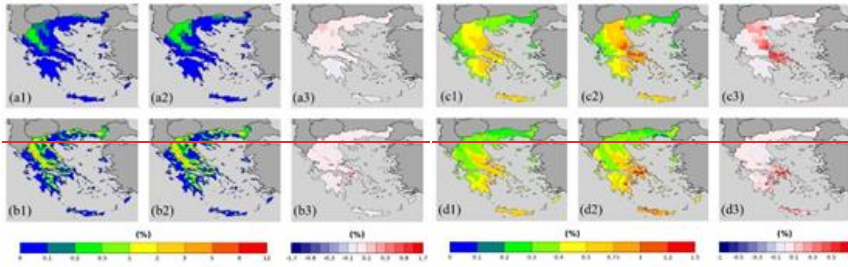
489

490 2. TX RR-WCCEs

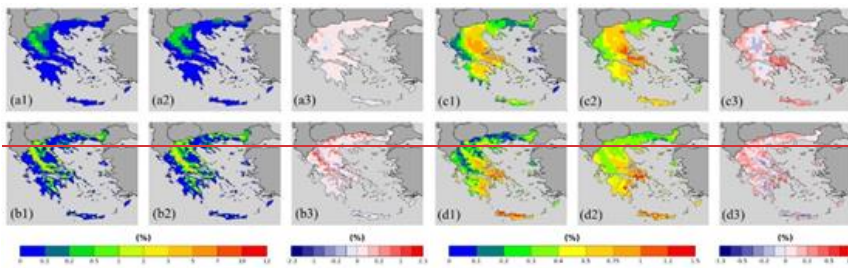
491



492 **Figure 22:** (a, b) RR20-ID and (c, d) RR95p-TX5p WCCEs probabilities. (a, c) ERA-5 and (b, d)
493 WRF-ERA-I. Column (1) is method A, (2) method B and (3) = (2) – (1).



494 **Figure 23:** (a, b) RR20-ID and (c, d) RR95p-TX5p WCCEs probabilities. (a, c) ERA-5 and (b, d)
495 WRF-ERA-I. Column (1) is method B, (2) method C and (3) = (2) – (1).



496 **Figure 24:** (a, b) RR20-ID and (c, d) RR95p-TX5p WCCEs probabilities. (a, c) ERA-5 and (b, d)
497 WRF-ERA-I. Column (1) is method A, (2) method C and (3) = (2) – (1).

498 Figures 22–24 show that RR20-ID events exhibit lower probabilities than RR20-FD events reaching
499 10% to 12%. RR95p-TX5p reach 1.5% at the most extreme values, which are distributed at a greater
500 area than RR95p-TN5p. On the other hand, method C exhibits the highest probabilities for both
501 approaches events.

502
503 **6. Past-Future Ensemble differencesProjections comparison**

504 We compare the historical period probabilities with the probabilities determined for the future
505 scenarios RCP 4.5 and RCP 8.5 for the 2025–2049 period by applying both fixed thresholds and
506 percentiles. This section displays the differences of the Ensemble mean WCCEs probabilities,
507 calculated for the empirical and the copula method, compared to the past probabilities presented in
508 the previous section. The differences mapped are statistically significant at 95% level using the
509 Student's t-test (Goulden, 1939) comparing 25 annual values of the timeseries. We have applied
510 the empirical method to calculate the probabilities of the WCCEs.

511 **6.1 RR20FD**

512 **1.**

513

Μορφοποιήθηκε: Πλήρης, Εσοχή: Αριστερά: 0 εκ.

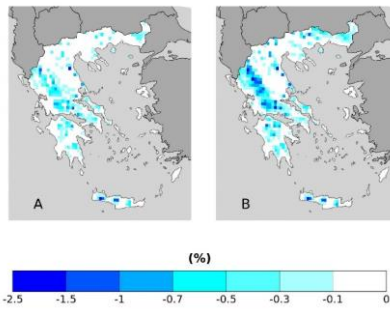
Μορφοποίησε: Γραμματοσειρά: Times New Roman, 10 στ., Έντονα

Μορφοποιήθηκε: Παράγραφος λίστας, Αριθμημένη διάρθρωση + Επίπεδο: 1 + Στυλ αριθμησης: 1, 2, 3, ... + Έναρξη από: 6 + Στοίχιση: Αριστερά + Στοίχιση: 0,63 εκ. + Εσοχή: 1,27 εκ.

Μορφοποιήθηκε: Πλήρης, Εσοχή: Αριστερά: 0,63 εκ.

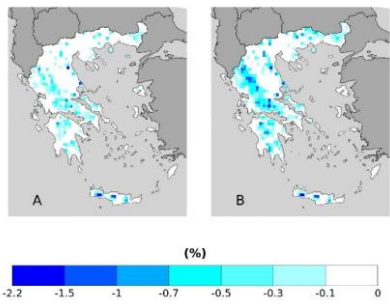
Μορφοποίησε: Γραμματοσειρά: Times New Roman, 10 στ.

Μορφοποιήθηκε: Εσοχή: Αριστερά: 1,27 εκ., Χωρίς κουκίδες ή αριθμηση



514

515 **Figure 12: RR20FD empirical method probability differences of future-past periods for (A)**
 516 **RCP4.5 and (B) RCP8.5 scenarios.**



517

518 **Figure 13: RR20FD copula method probability differences of future-past periods for (A) RCP4.5**
 519 **and (B) RCP8.5 scenarios.**

	<i>Empirical RCP4.5</i>	<i>Empirical RCP8.5</i>	<i>Copula RCP4.5</i>	<i>Copula RCP8.5</i>
<i>0<=Nc>-0.1</i>	34	31	64	57
<i>-0.1<=Nc>-0.3</i>	112	154	112	131
<i>-0.3<=Nc>-0.5</i>	63	65	53	81
<i>-0.5<=Nc>-0.7</i>	31	48	16	47
<i>-0.7<=Nc>-1</i>	12	34	6	24
<i>-1<=Nc>-1.5</i>	5	18	3	11
<i>Nc<=-1.5</i>	2	5	3	4
<i>MAX D</i>	-1.8063 %	-2.4988 %	-1.9500 %	-2.1392 %

520 **Table 7: ENSEMBLE Number of cells (Nc) in each category of probability difference (%) for**
 521 **RR20FD for empirical and copula method. MAX D denotes the maximum negative difference**
 522 **between future and past periods. Nv concerns only cells with statistically significant difference.**

523 From the results displayed in Figures 12 and 13 and in Table 7 RCP4.5 and RCP8.5 scenarios for the
 524 probabilities of the RR20FD events probabilities we observe that in all cases future scenarios yield only
 525 negative values meaning the reduction of RR20FD events in 2025-2049 period compared to 1980-2004
 526 period in all mountainous regions of Greece. RCP8.5 yields greater reduction of RR20FD probabilities
 527 than the RCP4.5 scenario both in spatial distribution and extreme values. The empirical method
 528 exhibits a greater reduction for the RCP8.5 scenario, although for RCP4.5 scenario both methods yield
 529 similar results.

Μορφοποίηση: Γραμματοσειρά: 9 στ., Αγγλικά (Ηνωμένων Πολιτειών)

Μορφοποίηση: Γραμματοσειρά: 9 στ.

Μορφοποιήθηκε: Στοιχισμένο στο κέντρο

Μορφοποιημένος πίνακας

Μορφοποίηση: Γραμματοσειρά: 9 στ., Αγγλικά (Ηνωμένων Πολιτειών)

Μορφοποίηση: Γραμματοσειρά: 9 στ.

Μορφοποιήθηκε: Στοιχισμένο στο κέντρο

Μορφοποίηση: Γραμματοσειρά: 9 στ., Αγγλικά (Ηνωμένων Πολιτειών)

Μορφοποίηση: Γραμματοσειρά: 9 στ.

Μορφοποιήθηκε: Στοιχισμένο στο κέντρο

Μορφοποίηση: Γραμματοσειρά: 9 στ., Αγγλικά (Ηνωμένων Πολιτειών)

Μορφοποίηση: Γραμματοσειρά: 9 στ.

Μορφοποιήθηκε: Στοιχισμένο στο κέντρο

Μορφοποίηση: Γραμματοσειρά: 9 στ., Αγγλικά (Ηνωμένων Πολιτειών)

Μορφοποίηση: Γραμματοσειρά: 9 στ.

Μορφοποιήθηκε: Στοιχισμένο στο κέντρο

Μορφοποίηση: Γραμματοσειρά: 9 στ.

Μορφοποιήθηκε: Στοιχισμένο στο κέντρο

Μορφοποίηση: Γραμματοσειρά: 9 στ.

Μορφοποιήθηκε: Στοιχισμένο στο κέντρο

Μορφοποίηση: Γραμματοσειρά: 9 στ., Αγγλικά (Ηνωμένων Πολιτειών)

Μορφοποίηση: Γραμματοσειρά: 9 στ.

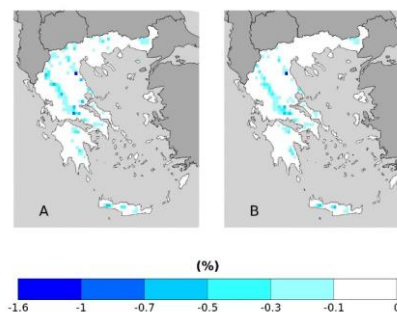
Μορφοποιήθηκε: Στοιχισμένο στο κέντρο

Μορφοποίηση: Γραμματοσειρά: 9 στ., Αγγλικά (Ηνωμένων Πολιτειών)

Μορφοποιήθηκε: Στοιχισμένο στο κέντρο

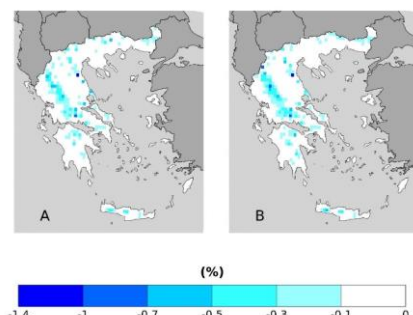
530

6.2 RR20ID



531

532 **Figure 14:** RR20ID empirical method probability differences of future-past periods for (A)
533 RCP4.5 and (B) RCP8.5 scenarios.



534

535 **Figure 15:** RR20ID copula method probability differences of future-past periods for (A) RCP4.5
536 and (B) RCP8.5 scenarios.

	<i>Empirical RCP4.5</i>	<i>Empirical RCP8.5</i>	<i>Copula RCP4.5</i>	<i>Copula RCP8.5</i>
<i>0<=Nc>-0.1</i>	193	229	166	210
<i>-0.1<=Nc>-0.3</i>	81	71	96	109
<i>-0.3<=Nc>-0.5</i>	23	20	33	37
<i>-0.5<=Nc>-0.7</i>	9	5	9	7
<i>-0.7<=Nc>-1</i>	1	0	1	3
<i>Nc<=-1</i>	1	1	1	1
<i>MAX D</i>	1.5536	1.0593	1.3425	1.1362

537 **Table 8:** ENSEMBLE Number of cells (Nc) in each category of probability difference (%) for
538 RR20ID for empirical and copula method. MAX D denotes the maximum negative difference
539 between future and past periods. Nv concerns only cells with statistically significant difference.

540 Similarly to RR20FD, RR20ID events probabilities yield only zero or negative differences compared to
541 the past for both scenarios. Empirical and copula methods yield similar results in distribution and
542 extreme values. For both methods, the RCP4.5 scenario tends to higher reduction of RR20ID
543 probabilities than RCP8.5 as observed in Table 8. The six projection models we previously evaluated,
544 are used here to study their behavior in the calculation of the probabilities of WCCEs. We compare the

Μορφοποίηση: Γραμματοσειρά: Times New Roman, 10 στ.

Μορφοποιήθηκε: Παράγραφος λίστας, Αριθμημένη διάρθρωση + Επίπεδο: 2 + Συλ αριθμησης: 1, 2, 3, ... + Έναρξη από: 2 + Στοίχιση: Αριστερά + Στοίχιση: 0,63 εκ. + Εσοχή: 1,27 εκ.

Μορφοποίηση: Γραμματοσειρά: Έντονα

Μορφοποίηση: Γραμματοσειρά: Έντονα

Μορφοποίηση: Γραμματοσειρά: Έντονα

Μορφοποίηση: Γραμματοσειρά: Έντονα

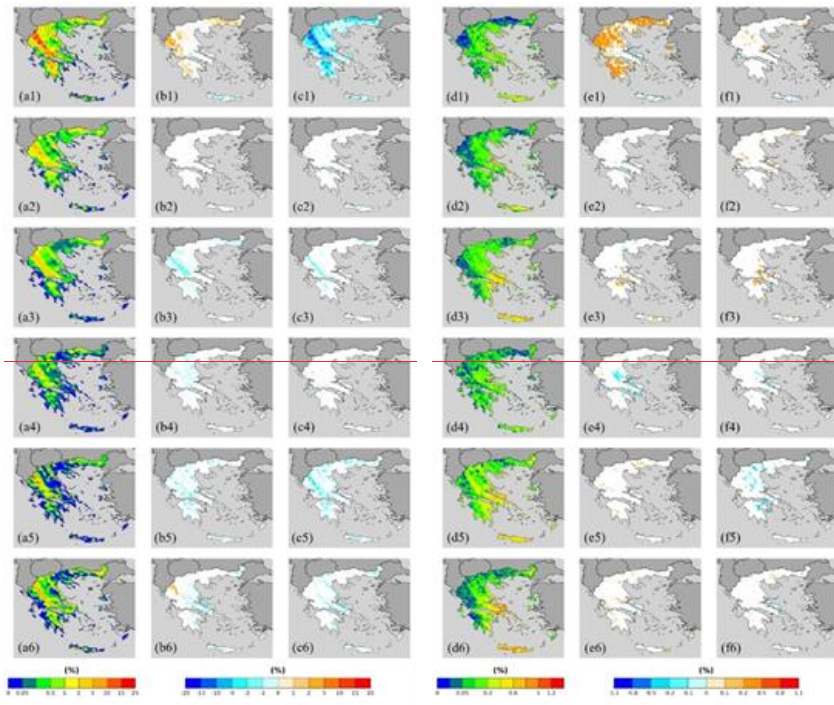
Μορφοποίηση

Μορφοποιημένος πίνακας

Μορφοποίηση

Μορφοποίηση: Αγγλικά (Ηνωμένων Πολιτειών)

545 historical period probabilities with the probabilities determined for the future scenarios RCP 4.5 and
 546 RCP 8.5 for the 2025–2049 period by applying both fixed thresholds and percentiles. The differences
 547 mapped are statistically significant at 95% level using the Student's t test (Goulden, 1939) comparing
 548 25 annual values of the timeseries. We have applied the empirical method to calculate the probabilities
 549 of the WCCEs. Univariate thresholds and probabilities are shown in Figures S4–S6 of the
 550 supplementary material.



551
 552 **Figure 25:** (a–c) RR20 FD and (d–f) RR95p TN5p probabilities. Models 1: CNRM, 2: KNMI, 3:
 553 CLMcom, 4: SMHI, 5: DMI, 6: WRF_EC. (a, d) 1980–2004, (b, e) (2025–2049 RCP 4.5)–(1980–
 554 2004) and (e, f) (2025–2049 RCP 8.5)–(1980–2004).

555 We see from Figure 25a that RR20 FD events probabilities may reach 25% particularly for CNRM,
 556 which also exhibits the greatest changes in the future, being mostly positive for RCP4.5 and extremely
 557 negative (up to –20%) for RCP8.5. Other models calculate fewer extreme probabilities for RR20 FD
 558 events and less extreme changes in the future being mostly negative and found in mountainous areas.
 559 RR95p TN5p events displayed in Figure 25d reach up to 1.5% only for WRF_EC. The rest of the
 560 models reach most extreme values in the range of 0.4% to 1%. Most models do not display significant
 561 changes in the future, except of CNRM which shows positive changes that spread extensively over
 562 Greece.

563 **Figure 26: (a-c) RR20-ID and (d-f) RR95p-TX5p probabilities. Models 1: CNRM, 2: KNMI, 3:**
564 **CLMcom, 4: SMHI, 5: DMI, 6: WRF_EC. (a, d) 1980-2004, (b, e) (2025-2049 RCP 4.5) – (1980-**
565 **2004) and (e, f) (2025-2049 RCP 8.5) – (1980-2004).**

566 Figure 26a shows that RR20-ID events are limited to mountainous areas. Again, CNRM exhibits in few
567 areas the most extreme values ranged between 10% to 20%. Similar values are, also exhibited by
568 WRF_EC. These models display the most extreme reduction of the probabilities in the future, reaching
569 10% to 15 % in the case of CNRM and RCP8.5. WRF_EC, DMI and to a lesser degree KNMI in
570 Figure 26d, yield the most extreme probabilities for RR95p-TX5p events that reach 1%. The most
571 notable changes are displayed by CNRM under RCP4.5, which shows increases in western and
572 northern parts of the country and significant decreases in eastern areas and Crete.

573 Conclusions

574 This work presents for the first time to our knowledge an extensive study of wet-cold compound events
575 in Greece for the historical and future periods of 1980-2004 and 2025-2049, respectively. Models' data
576 from the EUROCORDEX initiative of 0.11° resolution and reanalysis data (ERA5 and ERA-Interim
577 dynamically downscaled to 5km^2) were used and validated for the determined WCCEs against the
578 formally available observational datasets by HNMS for the country. The number of events and their
579 probabilities of occurrence were determined by applying two different approaches, fixed thresholds
580 approach_and_percentiles. Then, the bivariate validation of the models' datasets against observations
581 was performed for the determined bivariate thresholds (univariate and bivariate) and the 20 years
582 return levels using block maxima and POT methods. The probabilityprobabilities of WCCEs waswere
583 computed using the empirical method and the best-fitted copula for the bivariate timeseries for
584 observational data, reanalysis, projection models and the Ensemble of the projection models. Copulas
585 yield higher extreme events probabilities for most of the cases considering the dependence between

586 temperature and precipitation Moreover, for the reanalysis data, we applied the approach of the most
587 common copula of the 21 observational stations.

588 Even though reanalysis and projection models seemed to underestimate extreme precipitation, thus
589 leading to less extreme events, both helped to map the geographical distribution of WCCEs over
590 Greece. All models agreed that for the historical period, more events by the fixed threshold approach
591 were found over mountainous regions while the percentile approach yielded more WCCEs over the
592 eastern parts of the country and Crete. Although, there is an absence of stations over mountainous areas
593 we trust the results produced by models since bivariate validation shows good agreement between
594 observations and models. This trust is enhanced by the fact that winter period systems that affect large
595 areas crossing the country from north to south or from west to east (Cartalis et al., 2010) and therefore
596 recorded by available stations. Also, in the cold period of the year convective precipitation forced by
597 orography is limited hence the doubt that the models do not simulate extreme rainfall in winter is
598 reduced. Moreover, the use of the Ensemble mean of the models reduces the probability of models'
599 overestimation or underestimation of extreme events occurrences.

600 Furthermore, the projected changes in the number of WCCEs were investigated under RCP 4.5 and
601 RCP 8.5. Significant changes were obtained using the fixed threshold method over mountainous areas
602 which showed a potential reduction of the number of compound events particularly under RCP 8.5. The
603 application of the percentile method yielded reduced changes in the probabilities of wet-cold
604 compounds than the fixed threshold approach while the models showcased higher disagreement among
605 them concerning the changes.

606 The reduction of RR20-FD and RR20-ID WCCEs on mountains that the Ensemble of most projection
607 models predicted for predict in the future, might mean contribute to less heavy snowfall events and
608 possibly less accumulated snow depth. If such a scenario will be verified, Greece faces the threat of
609 losing the main sources of fresh water that come from melted mountain snow during spring or early
610 summer in the near future. The rise of temperature due to global warming is the main factor for the
611 reduction of WCCEs (Supplementary Figures S5-S7), thus similar mountainous regions in other parts
612 of the planet face similar danger considering the unique characteristics of each area. The change of
613 WCCEs for RR95p (TN5p or TX5p) does not necessarily translate to a corresponding change of
614 snowfall events, since the temperature percentile thresholds are for several occasions higher than 0 °C.
615 Snow events may occur at higher temperatures, however in this study we examined the amount of
616 precipitation and not its type. Next future steps could focus on the investigation of the synoptic systems
617 that cause wet cold compound events in the area of interest. The higher resolution reanalysis and
618 projection simulations used in the study, WRF ERA-I and WRF EC, exhibited with greater detail the
619 distribution of WCCEs, highlighting the need for high resolution model data for areas with diverse
620 topography like Greece.

621

622 Acknowledgments

623 The authors acknowledge partial funding by the project “National Research Network for Climate
624 Change and its Impacts, (CLIMPACT - 105658/17-10-2019)” of the Ministry of Development, GSRT,
625 Program of Public Investment, 2019.

626 References

- 627 Abdi, H.: The Kendall Rank Correlation Coefficient, 2007.
- 628 Abraj, M. A. M. and Hewaarachchi, A. P.: Joint return period estimation of daily maximum and
629 minimum temperatures using copula method, 66, 175–190, <https://doi.org/10.17654/AS066020175>,
630 2021.
- 631 Aghakouchak, A., Chiang, F., Huning, L. S., Love, C. A., Mallakpour, I., Mazdiyasni, O., Moftakhari,
632 H., Papalexiou, S. M., Ragno, E., and Sadegh, M.: Climate Extremes and Compound Hazards in a
633 Warming World, 48, 519–548, <https://doi.org/10.1146/ANNUREV-EARTH-071719-055228>, 2020.

- 634 Akaike, H.: A New Look at the Statistical Model Identification, 19, 716–723,
635 https://doi.org/10.1109/TAC.1974.1100705, 1974.
- 636 Anagnostopoulou, C. and Tolika, K.: Extreme precipitation in Europe: Statistical threshold selection
637 based on climatological criteria, 107, 479–489, https://doi.org/10.1007/S00704-011-0487-
638 8/TABLES/2, 2012.
- 639 Balkema, A. A. and Haan, L. de: Residual Life Time at Great Age, 2, 792–804,
640 https://doi.org/10.1214/AOP/1176996548, 1974.
- 641 [Boumier, E.: Peaks Over Threshold Modelling of Environmental Data, 2014.](#)
- 642 [Cartalis, C., Chrysoulakis, N., Feidas, H., and Pitsikas, N.: International Journal of Remote Sensing](#)
643 [Categorization of cold period weather types in Greece on the basis of the photointerpretation of](#)
644 [NOAA/AVHRR imagery Categorization of cold period weather types in Greece on the basis of the](#)
645 [photointerpretation of NOAA/AVHRR imagery, https://doi.org/10.1080/01431160310001632684,](#)
646 [2010.](#)
- 647 [Cardoso, R. M., Soares, P. M. M., Lima, D. C. A., and Miranda, P. M. A.: Mean and extreme](#)
648 [temperatures in a warming climate: EURO CORDEX and WRF regional climate high-resolution](#)
649 [projections for Portugal, 52, 129–157, https://doi.org/10.1007/S00382-018-4124-4/FIGURES/8, 2019.](#)
- 650 Christensen, O. B.: Regional climate change in Denmark according to a global 2-degree-warming
651 scenario, 2006.
- 652 [Chukwudum, Q. C. and Nadarajah, S.: Bivariate Extreme Value Analysis of Rainfall and Temperature](#)
653 [in Nigeria, Environmental Modeling and Assessment, 27, 343–362, https://doi.org/10.1007/S10666-](#)
654 [021-09781-7/TABLES/13, 2022.](#)
- 655 Coles, S.: An Introduction to Statistical Modeling of Extreme Values, https://doi.org/10.1007/978-1-
656 4471-3675-0, 2001.
- 657 Cong, R. G. and Brady, M.: The interdependence between rainfall and temperature: Copula analyses,
658 2012, https://doi.org/10.1100/2012/405675, 2012.
- 659 Curtis, S., Fair, A., Wistow, J., Val, D. v., and Owen, K.: Impact of extreme weather events and climate
660 change for health and social care systems, 16, 23–32, https://doi.org/10.1186/S12940-017-0324-
661 3/METRICS, 2017.
- 662 [de Luca, P., Messori, G., Faranda, D., Ward, P. J., and Coumou, D.: Compound warm-dry and cold-wet](#)
663 [events over the Mediterranean, 11, 793–805, https://doi.org/10.5194/ESD-11-793-2020, 2020.](#)
- 664 Demiroglu, O. C., Kučerová, J., and Ozcelebi, O.: Snow reliability and climate elasticity: Case of a
665 Slovak ski resort, 70, 1–12, https://doi.org/10.1108/TR-01-2014-0003/FULL/PDF, 2015.
- 666 Dzupire, N. C., Ngare, P., and Odongo, L.: A copula based bi-variate model for temperature and
667 rainfall processes, 8, e00365, https://doi.org/10.1016/J.SCIAF.2020.E00365, 2020.
- 668 Fisher, R. A. and Tippett, L. H. C.: Limiting forms of the frequency distribution of the largest or
669 smallest member of a sample, 24, 180–190, https://doi.org/10.1017/S0305004100015681, 1928.
- 670 Fonseca, D., Carvalho, M. J., Marta-Almeida, M., Melo-Gonçalves, P., and Rocha, A.: Recent trends of
671 extreme temperature indices for the Iberian Peninsula, 94, 66–76,
672 https://doi.org/10.1016/J.PCE.2015.12.005, 2016.
- 673 García-Ruiz, J. M., López-Moreno, I. I., Vicente-Serrano, S. M., Lasanta-Martínez, T., and Beguería,
674 S.: Mediterranean water resources in a global change scenario, 105, 121–139,
675 https://doi.org/10.1016/J.EARSCIREV.2011.01.006, 2011.
- 676 Gilleland, E. and Katz, R. W.: extRemes 2.0: An Extreme Value Analysis Package in R, 72, 1–39,
677 https://doi.org/10.18637/JSS.V072.I08, 2016.

- 678 Gnedenko, B.: Sur La Distribution Limite Du Terme Maximum D'Une Serie Aleatoire, 44, 423,
679 https://doi.org/10.2307/1968974, 1943.
- 680 Goda, Y.: Inherent Negative Bias of Quantile Estimates of Annual Maximum Data Due to Sample Size
681 Effect: A Numerical Simulation Study, 53, 397–429, https://doi.org/10.1142/S0578563411002409,
682 2018.
- 683 Goulden, C.: Methods of statistical analysis., 1939.
- 684 Hao, Z., Singh, V. P., and Hao, F.: Compound Extremes in Hydroclimatology: A Review, 10, 718,
685 https://doi.org/10.3390/W10060718, 2018.
- 686 Hersbach, H., Bell, B., Berrisford, P., Hirahara, S., Horányi, A., Muñoz-Sabater, J., Nicolas, J., Peubey,
687 C., Radu, R., Schepers, D., Simmons, A., Soci, C., Abdalla, S., Abellán, X., Balsamo, G., Bechtold, P.,
688 Biavati, G., Bidlot, J., Bonavita, M., de Chiara, G., Dahlgren, P., Dee, D., Diamantakis, M., Dragani,
689 R., Flemming, J., Forbes, R., Fuentes, M., Geer, A., Haimberger, L., Healy, S., Hogan, R. J., Hólm, E.,
690 Janisková, M., Keeley, S., Laloyaux, P., Lopez, P., Lupu, C., Radnoti, G., de Rosnay, P., Rozum, I.,
691 Vamborg, F., Villaume, S., and Thépaut, J. N.: The ERA5 global reanalysis, 146, 1999–2049,
692 https://doi.org/10.1002/QJ.3803, 2020.
- 693 Hochman, A., Marra, F., Messori, G., Pinto, J., Raveh-Rubin, S., Yosef, Y., and Zittis, G.: ESD
694 Reviews: Extreme Weather and Societal Impacts in the Eastern Mediterranean, 1–53,
695 https://doi.org/10.5194/ESD-2021-55, 2021.
- 696 Houston, T. G., Changnon, S. A., Ae, T. G. H., and Changnon, S. A.: Freezing rain events: a major
697 weather hazard in the conterminous US, 40, 485–494, https://doi.org/10.1007/S11069-006-9006-0,
698 2006.
- 699 James Pickands: Statistical Inference Using Extreme Order Statistics, 3, 119–131,
700 https://doi.org/10.1214/AOS/1176343003, 1975.
- 701 Konisky, D. M., Hughes, L., and Kaylor, C. H.: Extreme weather events and climate change concern,
702 134, 533–547, https://doi.org/10.1007/S10584-015-1555-3/FIGURES/3, 2016.
- 703 Kundzewicz, Z. W., Radziejewski, M., and Pińskwar, I.: Precipitation extremes in the changing climate
704 of Europe, 31, 51–58, https://doi.org/10.3354/CR031051, 2006.
- 705 Lazoglou, G. and Anagnostopoulou, C.: Joint distribution of temperature and precipitation in the
706 Mediterranean, using the Copula method, 135, 1399–1411, https://doi.org/10.1007/S00704-018-2447-
707 Z/FIGURES/5, 2019.
- 708 Lemos-Canovas, M.: Changes in compound monthly precipitation and temperature extremes and their
709 relationship with teleconnection patterns in the Mediterranean, Journal of Hydrology, 608, 127580,
710 https://doi.org/10.1016/J.JHYDROL.2022.127580, 2022.
- 711 Leonard, M., Westra, S., Phatak, A., Lambert, M., van den Hurk, B., McInnes, K., Risbey, J., Schuster,
712 S., Jakob, D., and Stafford-Smith, M.: A compound event framework for understanding extreme
713 impacts, 5, 113–128, https://doi.org/10.1002/WCC.252, 2014.
- 714 Lhotka, O. and Kyselý, J.: Precipitation–temperature relationships over Europe in CORDEX regional
715 climate models, International Journal of Climatology, https://doi.org/10.1002/JOC.7508, 2021.
- 716 Llasat, M. C., Turco, M., Quintana-Seguí, P., and Llasat-Botija, M.: The snow storm of 8 March 2010
717 in Catalonia (Spain): a paradigmatic wet-snow event with a high societal impact, 14, 427–441,
718 https://doi.org/10.5194/NHESS-14-427-2014, 2014.
- 719 de Luca, P., Messori, G., Faranda, D., Ward, P. J., and Coumou, D.: Compound warm-dry and cold-wet
720 events over the Mediterranean, 11, 793–805, https://doi.org/10.5194/ESD-11-793-2020, 2020.
- 721 Markantonis, I., Vlachogiannis, D., Sfetsos, T., Kioutsioukis, I., and Politi, N.: An Investigation of
722 cold-wet Compound Events in Greece, https://doi.org/10.5194/EMS2021-188, 2021.

- 723 van Meijgaard, E., van Ulft, L. H., van de Berg, W. J., Bosveld, F. C., van den Hurk, B. J. J. M.,
 724 Lenderink, G., and Siebesma, A. P.: The KNMI regional atmospheric climate model RACMO version
 725 2.1, 2008.
- 726 Moalafhi, D. B., Evans, J. P., and Sharma, A.: Evaluating global reanalysis datasets for provision of
 727 boundary conditions in regional climate modelling, 47, 2727–2745, <https://doi.org/10.1007/S00382-016-2994-X/TABLES/9>, 2016.
- 729 Moberg, A., Jones, P. D., Lister, D., Walther, A., Brunet, M., Jacobbeit, J., Alexander, L. v., Della-
 730 Marta, P. M., Luterbacher, J., Yiou, P., Chen, D., Tank, A. M. G. K., Saladié, O., Sigró, J., Aguilar, E.,
 731 Alexandersson, H., Almarza, C., Auer, I., Barriendos, M., Begert, M., Bergström, H., Böhm, R., Butler,
 732 C. J., Caesar, J., Drebs, A., Founda, D., Gerstengarbe, F. W., Micela, G., Maugeri, M., Österle, H.,
 733 Pandzic, K., Petrakis, M., Srnec, L., Tolasz, R., Tuomenvirta, H., Werner, P. C., Linderholm, H.,
 734 Philipp, A., Wanner, H., and Xoplaki, E.: Indices for daily temperature and precipitation extremes in
 735 Europe analyzed for the period 1901–2000, 111, 22106, <https://doi.org/10.1029/2006JD007103>, 2006.
- 736 Nelsen, R.: An introduction to copulas, 2007.
- 737 Pandey, P. K., Das, L., Jhajharia, D., and Pandey, V.: Modelling of interdependence between rainfall
 738 and temperature using copula, 4, 867–879, <https://doi.org/10.1007/S40808-018-0454-9>, 2018.
- 739 Pestereva, N. M., Popova, N. Yu., and Shagarov, L. M.: Modern Climate Change and Mountain Skiing
 740 Tourism: the Alps and the Caucasus, 1602–1617, 2012.
- 741 Politi, N., Nastos, P. T., Sfetsos, A., Vlachogiannis, D., and Dalezios, N. R.: Evaluation of the AWR-
 742 WRF model configuration at high resolution over the domain of Greece, 208, 229–245,
 743 <https://doi.org/10.1016/J.ATMOSRES.2017.10.019>, 2018.
- 744 Politi, N., Sfetsos, A., Vlachogiannis, D., Nastos, P. T., and Karozis, S.: A Sensitivity Study of High-
 745 Resolution Climate Simulations for Greece, 8, 44, <https://doi.org/10.3390/CLI8030044>, 2020.
- 746 Politi, N., Vlachogiannis, D., Sfetsos, A., and Nastos, P. T.: High-resolution dynamical downscaling of
 747 ERA-Interim temperature and precipitation using WRF model for Greece, 57, 799–825,
 748 <https://doi.org/10.1007/S00382-021-05741-9/FIGURES/17>, 2021.
- 749 Politi, N., Vlachogiannis, D., Sfetsos, A., Nastos, P.T., High resolution projections for extreme
 750 temperatures and precipitation over Greece, under review, <https://doi.org/10.21203/rs.3.rs-1263740/v1>,
 751 2022
- 752 Pongrácz, R., Bartholy, J., Gelybó, G., and Szabó, P.: Detected and expected trends of extreme climate
 753 indices for the carpathian basin, 15–28, https://doi.org/10.1007/978-1-4020-8876-6_2, 2009.
- 754 ~~754 Poschlad, B.: Using high-resolution regional climate models to estimate return levels of daily extreme
 755 precipitation over Bavaria, 21, 3573–3598, <https://doi.org/10.5194/NHESS-21-3573-2021>, 2021.~~
- 756 Raziei, T., Daryabari, J., Bordi, I., Modarres, R., and Pereira, L. S.: Spatial patterns and temporal trends
 757 of daily precipitation indices in Iran, 124, 239–253, <https://doi.org/10.1007/S10584-014-1096-1/TABLES/1>, 2014.
- 759 Rockel, B., Will, A., and Hense, A.: The regional climate model COSMO-CLM (CCLM), 17, 347–348,
 760 <https://doi.org/10.1127/0941-2948/2008/0309>, 2008.
- 761 Sadegh, M., Moftakhar, H., Gupta, H. v., Ragno, E., Mazdiyasni, O., Sanders, B., Matthew, R., and
 762 AghaKouchak, A.: Multihazard Scenarios for Analysis of Compound Extreme Events, 45, 5470–5480,
 763 <https://doi.org/10.1029/2018GL077317>, 2018.
- 764 Samuelsson, P., Jones, C. G., Willén, U., Ullerstig, A., Gollvik, S., Hansson, U., Jansson, C.,
 765 Kjellström, E., Nikulin, G., and Wyser, K.: The Rossby Centre Regional Climate model RCA3: model
 766 description and performance, 63, 4–23, <https://doi.org/10.1111/J.1600-0870.2010.00478.X>, 2016.

767 Schepsmeier, U., Stoeber, J., Christian, E., and Maintainer, B.: Package “VineCopula” Type Package
768 Title Statistical inference of vine copulas, 2013.

769 [Schwarz, G.: Estimating the Dimension of a Model, https://doi.org/10.1214/aos/1176344136, 6, 461–](https://doi.org/10.1214/aos/1176344136) 464, [https://doi.org/10.1214/AOS/1176344136, 1978.](https://doi.org/10.1214/AOS/1176344136)

Μορφοποιήθηκε: Αριστερά

Μορφοποίησε: Γραμματοσειρά:

771 Singh, H., Najafi, M. R., and Cannon, A. J.: Characterizing non-stationary compound extreme events in
772 a changing climate based on large-ensemble climate simulations, 56, 1389–1405,
773 <https://doi.org/10.1007/S00382-020-05538-2/FIGURES/6>, 2021.

774 Sklar and M.: Fonctions de repartition a n dimensions et leurs marges, 8, 229–231, 1959.

775 Spiridonov, V., Somot, S., and Déqué, M.: ALADIN-Climate: from the origins to present date, n.d.

776 Tavakol, A., Rahmani, V., and Harrington, J.: Probability of compound climate extremes in a changing
777 climate: A copula-based study of hot, dry, and windy events in the central United States, 15, 104058,
778 <https://doi.org/10.1088/1748-9326/ABB1EF>, 2020.

779 Tošić, I. and Unkašević, M.: Extreme daily precipitation in Belgrade and their links with the prevailing
780 directions of the air trajectories, 111, 97–107, <https://doi.org/10.1007/S00704-012-0647-5/FIGURES/9>,
781 2013.

782 [Tringa E and Kostopoulou E: An observational study of the relationships between extreme temperature](#)
783 [and precipitation and the surface atmospheric circulation in Greece, n.d.](#)

784 Trujillo, E., Molotch, N. P., Goulden, M. L., Kelly, A. E., and Bales, R. C.: Elevation-dependent
785 influence of snow accumulation on forest greening, 5, 705–709, <https://doi.org/10.1038/ngeo1571>,
786 2012.

787 Vajda, A., Tuomenvirta, H., Juga, I., Nurmi, P., Jokinen, P., and Rauhala, J.: Severe weather affecting
788 European transport systems: The identification, classification and frequencies of events, 72, 169–188,
789 <https://doi.org/10.1007/S11069-013-0895-4/TABLES/3>, 2014.

790 [van Meijgaard, E., van Ulft, L. H., van de Berg, W. J., Bosveld, F. C., van den Hurk, B. J. J. M.,](#)
791 [Lenderink, G., and Siebesma, A. P.: The KNMI regional atmospheric climate model RACMO version](#)
792 [2.1, 2008.](#)

793 Vogel, J., Paton, E., and Aich, V.: Seasonal ecosystem vulnerability to climatic anomalies in the
794 Mediterranean, 18, 5903–5927, <https://doi.org/10.5194/BG-18-5903-2021>, 2021.

795 [Voudouri, A. and Kotta, D.: Factors Determined Snow Accumulation Over the Greater Athens Area](#)
796 [During the Latest Snowfall Events, 355–361, https://doi.org/10.1007/978-3-642-29172-2_50](#), 2013.

797 Zanocco, C., Boudet, H., Nilson, R., Satein, H., Whitley, H., and Flora, J.: Place, proximity, and
798 perceived harm: extreme weather events and views about climate change, 149, 349–365,
799 <https://doi.org/10.1007/S10584-018-2251-X/TABLES/2>, 2018.

800 Zhang, W., Luo, M., Gao, S., Chen, W., Hari, V., and Khouakhi, A.: Compound Hydrometeorological
801 Extremes: Drivers, Mechanisms and Methods, 9, 941,
802 <https://doi.org/10.3389/FEART.2021.673495/BIBTEX>, 2021.

803 Zscheischler, J. and Seneviratne, S. I.: Dependence of drivers affects risks associated with compound
804 events, 3, https://doi.org/10.1126/SCIADV.1700263/SUPPL_FILE/1700263_SM.PDF, 2017.

805 Zscheischler, J., Orth, R., and Seneviratne, S. I.: Bivariate return periods of temperature and
806 precipitation explain a large fraction of European crop yields, 14, 3309–3320,
807 <https://doi.org/10.5194/BG-14-3309-2017>, 2017.

808 Zscheischler, J., Westra, S., van den Hurk, B. J. J. M., Seneviratne, S. I., Ward, P. J., Pitman, A.,
809 AghaKouchak, A., Bresch, D. N., Leonard, M., Wahl, T., and Zhang, X.: Future climate risk from
810 compound events, 8, 469–477, <https://doi.org/10.1038/s41558-018-0156-3>, 2018.

811 Zhou, S., Zhang, Y., Williams, A. P., and Gentine, P.: Projected increases in intensity, frequency, and
812 terrestrial carbon costs of compound drought and aridity events, *Science Advances*, 5,
813 https://doi.org/10.1126/SCIADV.AAU5740/SUPPL_FILE/AAU5740_SM.PDF, 2019.

Μορφοποίησε: Γραμματοσειρά: 10 στ., Όχι Έντονα

814 **Code and data availability**

815 Code and results data available upon request.

816 **Author contributions**

817 IM has worked on conceptualization, methodology, validation, visualization, investigation, writing
818 review and editing. AS, DV and IK contributed on conceptualization, review and supervision. All
819 authors have read and agreed to the published version of the manuscript.

820 **Competing interests**

821 The authors declare that they have no conflict of interest.

822

823 **Appendix A**

824

NUMBER	LOCATION	ID	LATITUDE	LONGITUDE	ELEVATION (m)
1	Alexandroupoli	16627	40.85	25.917	4
2	Elliniko	16716	37.8877	23.7333	10
3	Ioannina	16642	39.7	20.817	483
4	Irakleio	16754	35.339	25.174	39
5	Kalamata	16726	37.067	22.017	6
6	Kastoria	16614	40.45	21.28	660.95
7	Kerkira	16641	39.603	19.912	1
8	Kithira	16743	36.2833	23.0167	167
9	Larisa	16648	39.65	22.417	73
10	Limnos	16650	39.9167	25.2333	4
11	Methoni	16734	36.8333	21.7	34
12	Milos	16738	36.7167	24.45	183
13	Mitilini	16667	39.059	26.596	4
14	Naxos	16732	37.1	25.383	9
15	Rhodes	16749	36.42896	28.21661	95
16	Samos	16723	37.79368	26.68199	10
17	Skyros	16684	38.9676	24.4872	12
18	Souda	16746	35.4833	24.1167	151
19	Thessaloniki	16622	40.517	22.967	2
20	Tripoli	16710	37.527	22.401	651
21	Zakinthos	16719	37.751	20.887	5

825

826 **Table A1: HNMS stations information.**

827

828 **Appendix B**

← **Μορφοποιημένος πίνακας**

829

830 **Table B1: (-TN, RR) best-fitted Copula for each station timeseries.**

831



832

833



Μορφοποιημένος πίνακας

834 **Table B2: (-TX, RR) best-fitted Copula for each station timeseries.**